The Effect of Temperature on the Formation of Liesegang Patterns of Copper(II) chromate in Polyacrylamide Gels

A THESIS SUBMITTED TO
THE GRADUATE SCHOOL OF ENGINEERING AND SCIENCE
OF BILKENT UNIVERSITY
IN PARTIAL FULFILLMENT OF THE REQUIREMENTS
FOR
THE DEGREE OF
MASTER OF SCIENCE
IN CHEMISTRY

By
Muhammad Turab Ali Khan
September 2020

The Effect of Temperature on the Formation of Liesegang Patterns of Copper(II) chromate in Polyacrylamide Gels

By Muhammad Turab Ali Khan

September 2020

We certify that we have read thesis and that in our opinion it is fully adequate, in scope and in quality, as a thesis for the degree of Master of Science.

_____
Bilge BAYTEKIN (Advisor)

_____
İrem Erel GÖKTEPE

_____
Ferdi KARADAŞ

_____
Istvan LAGZI

_____
Halil İbrahim OKUR

Approved for the Graduate School of Engineering and Science:

_____
Ezhan KARAŞAN
Director of the Graduate School

ABSTRACT

The Effect of Temperature on the Formation of Liesegang patterns of Copper(II) chromate in Polyacrylamide Gels

Muhammad Turab Ali Khan

M.S. in Chemistry

Advisor: Bilge BAYTEKIN

September 2020

Liesegang patterns (LPs) are a subclass of periodic precipitation patterns that result in a reaction-diffusion (RD) without convection. Since their discovery, LPs have been studied to understand the effect of different parameters such as electric field, magnetic field, or concentration of ions/ gels and to elucidate the mechanism of pattern formation. LPs are visual "complex sums" of the chemical reactions forming the patterns, the diffusion of the chemicals, and the physical changes in the reaction environment. Different physical environments produce different patterns and therefore the patterns formed can be used to ‘sense’ the physical environment, in which the patterns are formed – if the changing physical parameter of the environment is previously linked to the various patterns forming under these conditions. In this study, we aim to achieve an LP system ($CuCl_2$(outer electrolyte)/K_2CrO_4(inner electrolyte) in polyacrylamide gel) that senses temperature by monitoring concurrent pattern formation. First, we illustrate the visual differences in LPs occurring at different temperatures. We unveil the changes in the diffusion of ions, the reaction rate, and the precipitation threshold inside the gel media for LP forming at different temperatures. LP's behaviors under different temperature ramp conditions leading to a difference in pattern evolution in terms of spacing, width, and time laws are shown. Finally, we show that temperature provides a degree of freedom towards material design through RD.

ÖZET

Poliakrilamit Jellerde Bakır(II) Kromat Liesegang Desenlerinin Oluşumunda Sıcaklığın Etkisi

Muhammad Turab Ali Khan
M.S. in Chemistry
Advisor: Bilge BAYTEKIN
September 2020

Liesegang desenleri (LDler), konveksiyon olmayan tepkime-difüzyon (TD) sistemlerinde oluşan periyodik desenlerin alt gruplarından biridir. Bu desenlerin oluşumunu anlamaya yönelik çalışmalar desen oluşumundaki elektrik ve manyetik alan, jel ve iyon konsantrasyonu gibi değişik parametrelerin oluşuma nasıl etki ettiğini anlamak üzerine yoğunlaşmıştır. LDler, onları oluşturan kimyasal tepkimelerin, bu tepkimelerde yer alan kimyasalların difüzyonunun ve tepkime ortamındaki fiziksel değişikliklerin görsel ve "kompleks toplamları"dır. Değişik fiziksel ortamlar değişik LDlerin oluşumuna neden olduğundan - eğer bir fiziksel değişkenin desen oluşumuna etkisi daha önceden belirlenmişse - bir ortamdaki desen oluşumu desenin oluştuğu bu ortamda bu değişkenin değişimini takip etmekte kullanılabilir. Bu çalışmada, bir LD sisteminin bahsedilen şekilde sıcaklığı algılayan bir sistem olarak kullanılabileceğini göstermek için, bakır klorür ve potasyum kromat dış ve iç elektrolitleriyle poliakrilamit jellerde oluşturulan bir LD sistemi kullanıldı. İlk olarak, değişik sıcaklıklarda oluşan desenlerdeki görsel değişimler not edildi ve sistemlerdeki iyon difüzyonları, tepkime hızı ve çökelme eşik değerindeki değişiklikler belirlendi. Ayrıca desenlerin evriminde, sıcaklık değişimi hızının da aralık, kalınlık ve zaman gibi LD kurallarına etkisi gösterildi. Son olarak da, sıcaklığın TD ile malzeme tasarımında bir serbestlik derecesi olarak kullanılabileceği gösterildi.

Acknowledgments:

I will always be grateful to Dr. Bilge Baytekin for her wonderful supervision of my work. I would like to express my sincere gratitude and respect for her guidance, support, and patience. Through her vision and constructive criticism, Dr. Bilge Baytekin helped me polish my research abilities and scientific thinking. I am grateful to her for always motivating me, being open to new ideas, and providing a friendly group environment.

I am very grateful to Dr. Tarik Baytekin for his guidance and help throughout the course of my work. I would like to also thank Dr. Istvan Lagzi for his guidance and time. I highly appreciate the time and guidance of Dr. Ferdi Karadaş, Dr. Halil İbrahim Okur, and Dr. İrem Erel Göktepe.

I am very grateful to be a part of a vibrant and progressive group. I would like to thank Mohammad Morsali for introducing me to the subject, helping me in the experiments, and for being a wonderful friend. I am sincerely grateful to Dr. Joanna Kwiczak Yigitbaşi for her help in the experiments, constructive guidance, and warm welcoming nature. I would like to thank Mine Demir for being supportive during my time in Bilkent and being an amazing friend. I am very grateful to Doruk Cezan for introducing me to Dr. Bilge Baytekin's work, for his motivational thoughts, and training me for initial experiments. I would also like to thank Pedram Tootoonchian for his assistance in the experiments. I would also like to thank Mertcan Özel, Dr. Fatma Demir, and Simay Aydonat for being supportive friends and assistance in the experiments.

I am also very grateful to my family and friends for patiently supporting me during my time at Bilkent University.

Table of Contents

List of Figures

Chapter 1

1. Introduction:

Nature employs patterns in a sublime and intricate fashion [1]. The synthetic pattern formation has been studied not only to reveal the mechanisms behind patterns occurring in nature but also to employ the patterns in technological applications [2] [3]. An important class of pattern forming systems, known as Liesegang patterns (LPs), was first discovered more than a century ago by R.E. Liesegang [4]. LPs are periodic precipitation patterns resulting from reaction-diffusion [5].The occurrence LPs is not limited to laboratory conditions. They have been reported to be occurring in tree trunks and volcanic rocks [6]. Since their discovery, studies have been carried out to build a universal model for LPs and to understand the experimental conditions for different LP systems. A typical experimental set involves two 'electrolytes' and a media. An outer electrolyte diffuses into the media, in which inner electrolyte is homogeneously distributed. LPs arise due to the reaction between the two electrolytes coupled with diffusion [7]. Different porous media have been reported to have patterned with LPs [8] [9]. Since most of the reactions chosen for LP formation occur in aqueous media, and for the formation of the LP convection has to be eliminated, hydrogels have thus far been mostly used as a suitable media for LP formation.

There are different models used to describe how LPs occur [10]. All of these models fall in two distinct categories; pre-nucleation models and post-nucleation models. Pre-nucleation explains LPs occurrence as a relaxation to an equilibrium state. It exerts on the fact that diffusive flux coupled with reaction results in a system far-from its equilibrium followed by the occurrence of a precipitation band as the system tends away from this non-equilibrium state. On the other hand, post-nucleation model suggests that due to the reaction between the two electrolytes, sol of the precipitate forms with distribution across

the media and LPs start to form later on. The occurrence of the precipitation band is not limited to the area of the colloid formation but the aggregation of larger particles (Ostwald supersaturation).

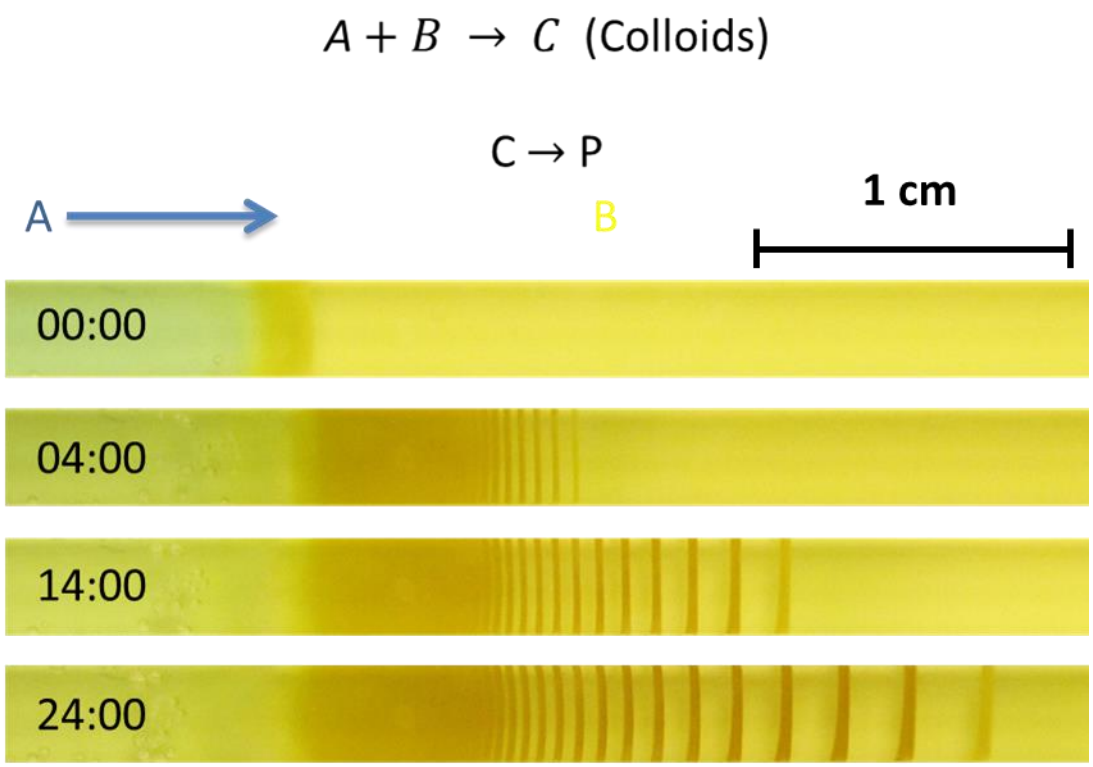

Figure 1: (top) The reaction equation resulting in the formation of LPs. A and B are the counter electrolytes; outer and inner, respectively. C refers to the colloids being produced and the aggregation of the colloids results in the precipitation bands, P (dark bands appearing in the photos below), according to the post-nucleation model. (bottom) The photos of an LP system showing the time evolution of patterns, where **A** (1 M copper chloride solution) diffuses in to the polyacrylamide hydrogel containing homogeneously distributed **B** (0.01 M potassium chromate) resulting in the precipitation bands, P, of copper(II) chromate. **A** is diffusing from left to right in all photos. Scale bar= 1 cm. Time is shown in hours.

Outer electrolyte A reacts with inner electrolyte B and this results in the formation of colloids, C which then nucleate to produce P (figure 1). The precipitation product appears

as visually distinct regions in the medium, e.g., in the system shown in Figure 1, they are the dark stripes in the photos of the system. LPs follow a set of mathematical laws, defined as spacing law [11], time law [12], and width law [13] (figure 2). Periodic precipitation bands form a geometric series and in most cases the distance between the patterns is increasing, i.e., an ascending series in terms of the spacing between the bands. For some systems, a descending series has been observed as well [14]. The first is called normal banding, while the latter is referred to as revert (inverse) banding phenomenon. The spacing between consecutive bands is characterized by the spacing law. Similarly, the width of the bands increases from beginning of precipitation to the end (width law). The last empirical law satisfied by Liesegang phenomenon, called as the time law, illustrates that LP formation follows diffusion-controlled kinetics [15].

Spacing Law: $1+p=\frac{X_{n+1}}{X_n}$ Time Law: $X_n = \sqrt{t}$ Width Law: $Q=\frac{W_{n+1}}{W_n}$

Figure 2: Mathematical relationships of spacing law, width law and time law with respect to the position of Liesegang patterns are shown. $\mathbf{X_n}$ refers to the distance (position) of the band with respect to the source of outer electrolyte. $\mathbf{X_{n+1}}$ refers to the position of the next consecutive band (spacing law). Similarly, $\mathbf{W_n}$ refers to the width of the band and $\mathbf{W_{n+1}}$ refers to the width of the next consecutive band (width law). Time law draws a relationship between the positions ($\mathbf{X_n}$) of the band with respect the time ($\mathbf{t}$) at which band starts to form.

1.1. Pattern Formation and The Reaction Environment

Pattern formation occurs in non-equilibrium systems with the interplay of reaction-diffusion [2]. In these systems, there are chains of complex events and the sum of these complex events form the visual patterns. There is an enormous potential for pattern forming systems to be employed in sensing technologies [16]. Any changes in the physical parameters directly affect these complex events and leave an 'impact' on the visual sums (patterns). Figure 3 (right) illustrates how dynamic patterns in the form of calcium waves enter retinal cells upon mechanical stimulation [2]. Such examples illustrate that patterns do possess the ability to reveal information about the surroundings. Another classic example would be tree rings [17] (figure 3: left). The morphology of the tree rings reveals information about the seasonal temperature changes in the surroundings and in certain cases, they also reveal the incline growth of the trees. The study of tree ring patterns is known as dendrochronology. It is the science of studying tree-trunk patterns to understand the changes in climatic and atmospheric conditions during the tree growth.

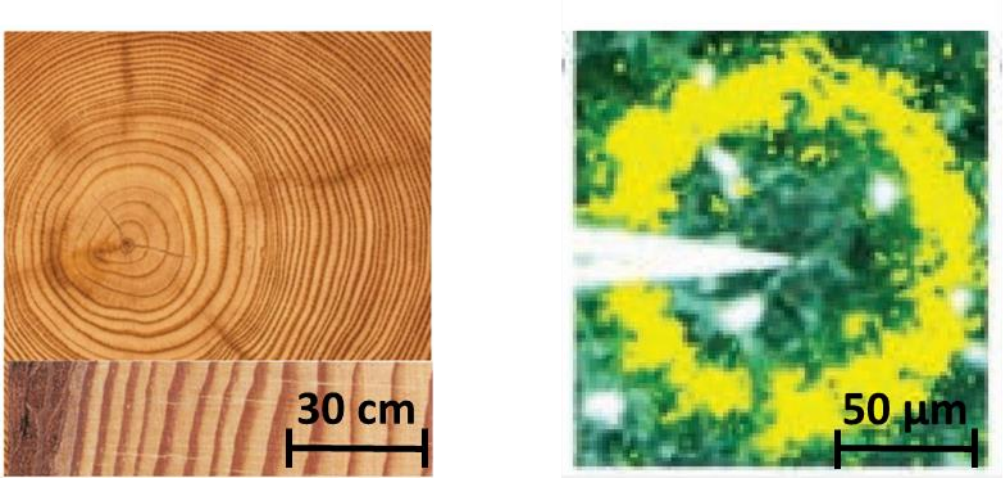

Figure 3: (Left) Cross-section of a tree trunk with distinguishable tree rings. (Right) Ca waves entering a retinal cell upon mechanical stimulation, reproduced from Grzybowski, 'Chemistry in motion'[2].

In our previous study [16], we illustrated how mechanical deformation can be tracked based on the evolution of the periodic precipitates. LPs form in both loaded (deformed)

and unloaded (no deformation) samples (figure 4). LPs shown in 4A were formed in the hydrogel undergoing zero percent stretch, while 4B demonstrates how LPs appear in a 40% loaded (stretched) sample after unloading. Furthermore, LPs were also able to signal the instances of the elastic deformation (figure 4C). The occurrence of the equidistant patterns (EP) upon the removal of the load marks the instance of unloading. Upon unloading the sample, there is a change in the flux of outer electrolyte (an increased concentration at that point) leading to production of EPs. This technique was employed to understand not only the extent of deformation, but also the time and duration of the deformation was revealed in the visual appearance of LPs. Henceforth, the relationship between the environment and LPs is definitely optically visible.

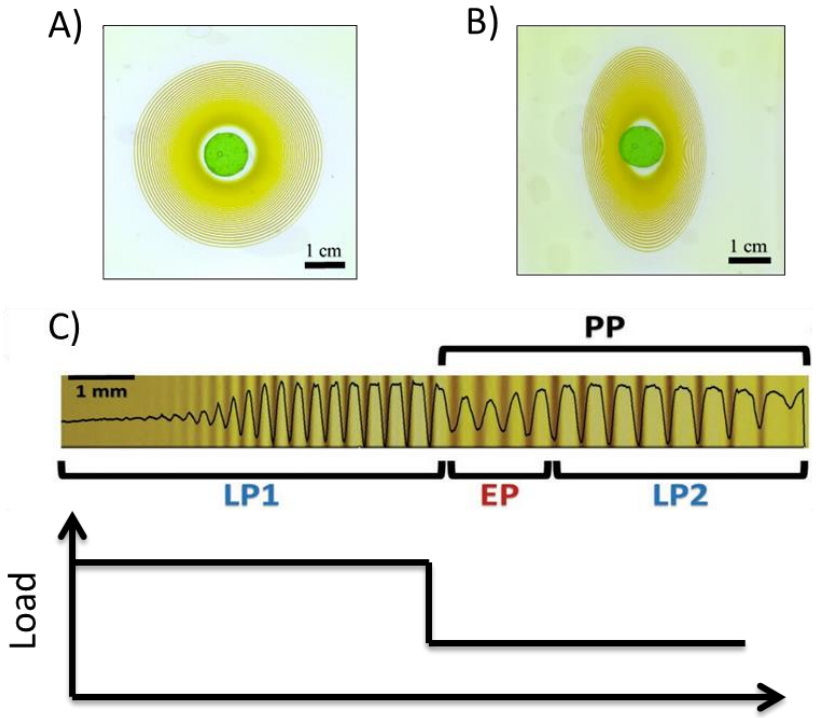

Figure 4: A) LPs formed in 2D arrays at 20^{o}C B) LPs formed in elastically deformed 2D array. C) Occurrence of the equidistant patterns (EP) when the load is removed i.e. no elastic deformation. EP bridges the two ascending series that exhibit Liesegang characteristics, LP1 and LP2 [16]. The system comprises of 1 M copper(II) chloride (outer electrolyte), 0.01 M potassium chromate (inner electrolyte) and polyacrylamide gel (media).

1.2. Factors Affecting LPs

Mechanically[16] probing LPs was the first study that exhibited how change of flux of ions can help achieve control over patterns. Previously, there have been studies related to understanding the effect of electric [18] and magnetic fields [19]. Along with, studies have been focused on understanding the effect of concentration of the electrolytes [20]. Different concentrations of the gels have also been studied as well as of the degree of cross-linking in gels [21] [22]. In this study, we have focused on understanding how patterns occur at different temperatures and whether LPs could visually mark the change of the environmental temperature.

1.3. Thermal Noise and Liesegang Patterns

Pattern forming chemical systems show astonishing figures and follow beautiful trends when studied at different temperatures [23] [24]. Temperature can be either used for quenching patterns or seeing different shapes [25]. Among all other factors, temperature is the only factor that affects reaction rate, diffusion coefficient and precipitation threshold at once [26]. Temperature has been reported as a factor for increasing the probability of helical patterns in cylindrical gels and alter pattern shape [27]. Earlier studies indicate that temperature affects diffusion coefficient and precipitation threshold [28]. Isemura's study revealed that temperature affects number of bands and the width of the depletion zone between the rings. The number of bands decreases and the spacing interval between the bands is reported to increase with temperature, in most cases. However, Popp's study showed that the bands were forming closer at higher temperatures [28]. These two contradictory observations are due to the difference in the solubility product's dependence on temperature. For instance, $Mg(OH)_2$ [28] is more soluble under cold conditions while Ag_2CO_3's [28] solubility increases with temperature. Another study indicated that no trend is observed in the spacing coefficient when experiments are conducted on specific temperatures [29]. However, all these studies are carried out in the temperature range of 0 to 30^{o}C. Han reported LPs at 40^{o}C that had higher spacing between them than at 30^{o}C, but the rings were broken at 40^{o}C [30]. The above-mentioned

studies involved Agarose and gelatin as the media of choice; above 45^{o}C agarose gel undergoes phase separation between its components [31] while gelatin melts over 30^{o}C, thus it becomes difficult to form and characterize LPs at temperatures higher than 40^{o}C. It is advised to keep the temperature low and constant to observe periodic precipitation in these gels [32]. However, Antal et al. also suggested that guiding fields, temperature or pH, can result in revert banding, equidistant banding and these guiding fields could be used for pattern control [33]. These characteristic bandings could be achieved by changing the flux of the ions. Nonetheless, no such experimental observation is reported in the literature with changing temperature.

Here we propose a study that quantifies the effect of temperature on Liesegang phenomenon. We show how temperature affects LPs of $CuCl_2$ (outer electrolyte)/K_2CrO_4 (inner electrolyte) in polyacrylamide gel. Polyacrylamide is a covalently cross-linked, stretchable hydrogel and its glass transition temperature is between 170 and 190^{o}C, depending on the degree of cross-linking [34]. Thus, Polyacrylamide gel acts as a thermally stable media for ambient temperatures (20 to 60^{o}C) considered in this study.

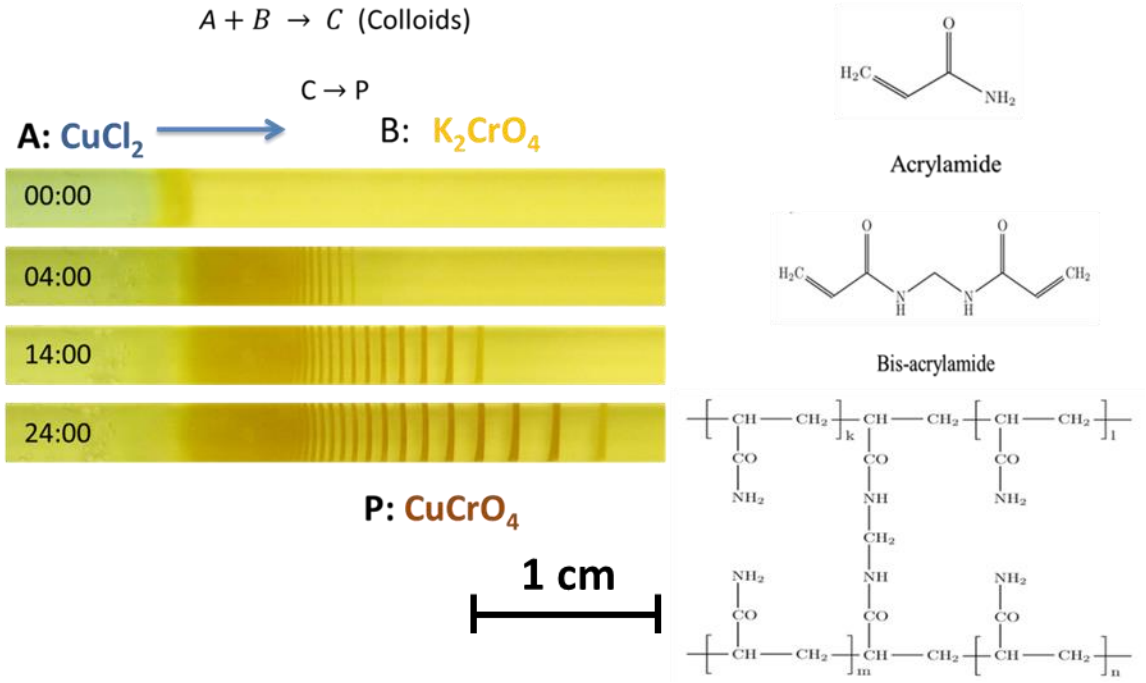

Figure 5: (Left) In our system, outer electrolyte, A, is 1 M copper(II) chloride, and 0.01 M potassium chromate is the inner electrolyte. Over the passage of time, we observe periodic precipitates of copper(II) chromate as dark lines. The diffusion of the outer electrolyte is from left to right in the photos. The time is given in hours. Scale bar is 1 cm. (Right) The hydrogel medium chosen in our experiments is polyacrylamide with bis-acrylamide as the cross-linker.

1.4. Pushed and Pulled fronts

A species diffuses into a media with a linearly spreading velocity. Periodic precipitation patterns occur in the wake of the reaction front [35]. It is logical to assume that faster moving fronts will produce patterns that will be different than patterns produced in the wake of a slower front. Similarly, if a continually flowing front at a certain velocity is disturbed, i.e. either accelerated or slowed down, there should be difference in the patterns in comparison to the patterns that would have formed without the change in velocity. The speed of the front is directly proportional to the temperature of the

surrounding as it directly affects the diffusion coefficient of the outer electrolyte. Thus, temperature can be a tool to alter the flow rates of the reaction front.

Upon heating up the system, it is expected that the flux of outer electrolytes will increase and the reaction front will experience a push. This is referred to as a pushed-front. On the other hand, when we cool down the system, the reaction front experiences a halt and hence, a pulled front. Theoretically it is proven that both coherent (with distinguishable trends) and incoherent patterns (chaotic) can result in the wake of pushed or pulled fronts. At this stage, we assume that LPs will demonstrate coherent patterns when temperature of the system is altered. The only difference between a pushed and pulled front is the occurrence of the relaxation time. Patterns immediately start to form in the wake of the pushed front, however, a pulled front system relaxes to a new initial condition and then patterns are observed [36]. With temperature variations, both pushed and pulled fronts could be monitored and pattern formation is to be observed, as the reaction front is accelerated or slowed down.

Chapter 2:

2. Materials and Methods:

2.1. Materials

Acrylamide (AA) (Sigma-Aldrich, 98 % purity), N,N'-methylene(bis)acrylamide (BIS) (Sigma-Aldrich, 99% purity), potassium peroxydisulfate (KPS) (Sigma-Aldrich, 99 % purity), N,N,N′,N′-tetramethylethylene-diamine (TEMED) (Sigma-Aldrich, 99% purity), potassium chromate (Merck, 99.5 %), copper(II) chloride dihydrate (Merck, 99 % purity), Methanol (Sigma-Aldrich, 99% purity)

Plexiglass and Parafilm® were used without any chemical modification.

2.2. Preparation of 1D, 2D, and 3D gels.

Molds for 1D, 2D, 3D and counter-diffusion experiments are designed in Adobe Illustrator and made from plexiglass using a laser cutter. 2 mm thick plexiglass sheet is used for all experiments, thus the thickness of the gels in 1D, 2D, and the counter-diffusion experiments is 2 mm as well.

2.2.1. 1D Gels:

Gel strips are prepared by mixing 0.723 grams of acrylamide, 0.003 grams of N, N'-methylenebisacrylamide (BIS), 0.01 g of potassium persulfate, and 0.01 g of potassium chromate as the inner electrolyte. A total of 4.8 ml of water is added to dissolve all the ingredients. The solution is ultrasonicated for 2 minutes. 10 microliters of tetramethylethylenediamine (TEMED), a free-radical initiator, is added to the gel

solution. The gel solution is then transferred to the mold and the top of the mold is closed by a piece of plexiglass. After approximately, 24 hours, 1 M $CuCl_2$ is introduced to the top of the gel. A small drop of oil is added on top of $CuCl_2$ solution inside the mold to reduce the evaporation of $CuCl_2$ solution. The gel is then placed horizontally, onto the home-built device (see below), which is adjusted to the desired temperature.

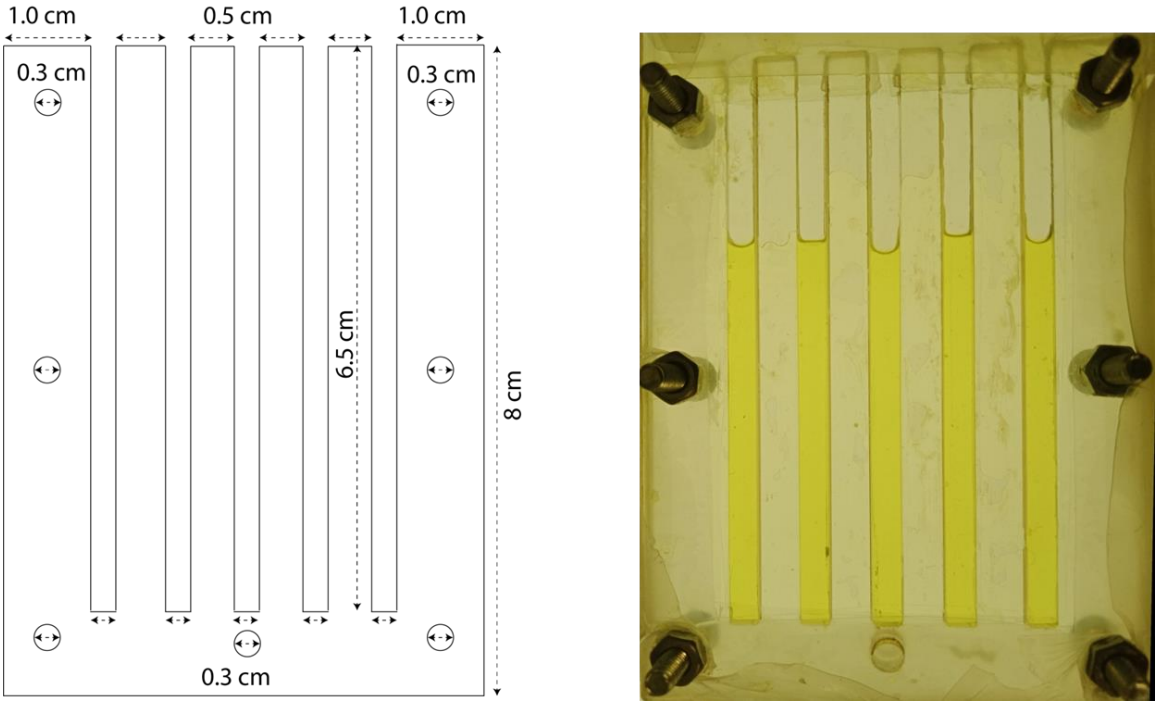

Figure 6: (Left) The dimensions of the spacer mold used for 1 D gels. The spacer mold is sandwiched between two plexiglass pieces with the 8 cm x 5.5 cm dimensions, using screws. (Right) the 1D gel samples (yellow) prior to the addition of the outer electrolyte are shown.

2.2.2. 2D gels:

1.446 grams of acrylamide, 0.006 grams of N, N'-methylenebisacrylamide, 0.02 g of potassium persulfate, and 0.02 g of potassium chromate as the inner electrolyte are dissolved in a total of 9.6 ml of water . The solution is ultrasonicated for 5 minutes. 10 microliters of tetramethylethylenediamine (TEMED), a free-radical initiator, is added to the gel solution. The gel solution is then transferred to the mold through the 'copper ions holder'. And the top of the holder is closed by a piece of Parafilm. After approximately, 24 hours, 1 M $CuCl_2$ is introduced to the top of the gel through the 'copper ions holder'. A small drop of oil is added on top of $CuCl_2$ solution inside the mold to reduce the evaporation of $CuCl_2$. The gel is then placed horizontally, onto the home-built device (see below), which is adjusted to the desired temperature.

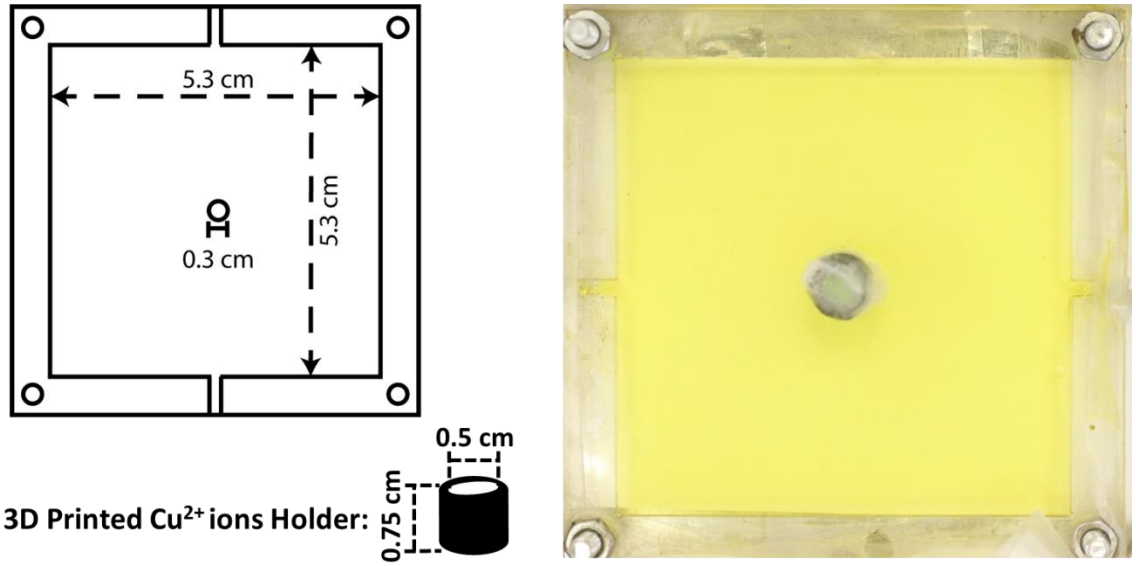

Figure 7: (Left) The dimensions of the mold for 2D gel sheets. The 'top' side has a hole of the diameter of 0.3 cm in the middle. The 3D printed Cu2+ holder is attached on top of the hole using Superglue. (Right) A 2D gel sheet (yellow) in the mold with the 'copper ions holder' prior to the addition of the outer electrolyte is shown. Thickness of the gel is 0.2 cm.

2.2.3. 3D gels:

3D blocks of gels are prepared in a plexiglass box (figure 8). The box is assembled and the outer edges are sealed with Ecoflex, to prevent any leakage. For a 3D block of PAM hydrogel, the precursor solution was scaled to 7 times of a 2D gel. 10.112 grams of acrylamide, 0.042 grams of N, N'-methylenebisacrylamide, 0.14 g of potassium persulfate, and 0.14 g of potassium chromate as an inner electrolyte. A total of 67.2 ml of water is added to dissolve all the ingredients. The solution is ultrasonicated for 5 minutes. 70 microliters of tetramethylethylenediamine (TEMED), a free-radical initiator, is added to the gel solution. The gel solution is then transferred to the plexiglass box through the 'copper ions holder' at the top. The top of the holder is closed by parafilm to reduce evaporation. After approximately, 24 hours, 1 M $CuCl_2$ is introduced to the top of the gel through the copper ions holder. A small drop of oil is added on top of $CuCl_2$ solution inside the mold to reduce the evaporation of $CuCl_2$. The 3D block of gel is then placed in an oil-bath set at the desired temperature.

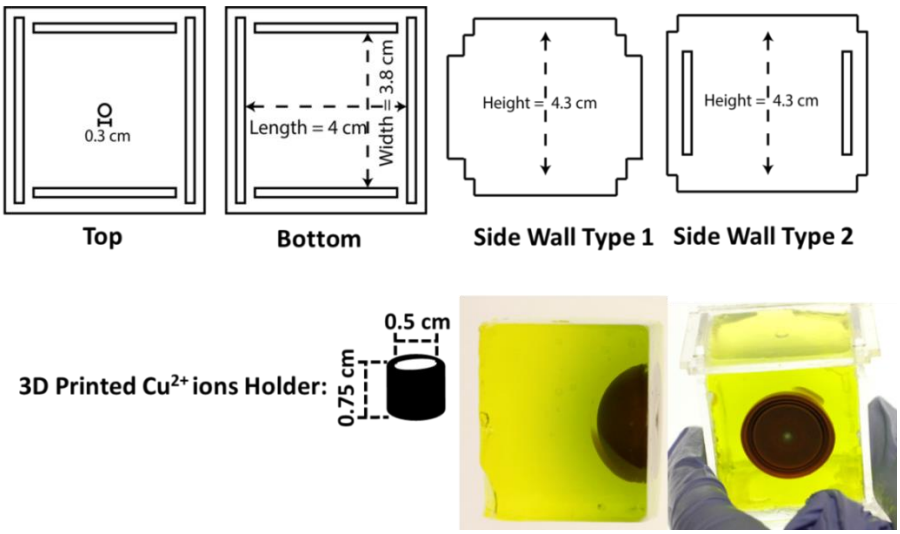

Figure 8: (Top) The dimensions for each of the sides of the cubical box. The pieces are fitted into one another and the edges are sealed from outside using Ecoflex. The 3D printed Cu^{2+} holder is attached to the top face of the cube. 3D samples with patterns formed inside the cubical box are shown at the bottom right.

2.3. Counter-Diffusion Experiments

A mold is designed to be capable of holding a 1 cm column of polyacrylamide hydrogel without any inner electrolyte. The molds are designed similarly to the 1D gel, i.e., a spacer mold of height 0.2 cm is sandwiched between two plexiglass pieces of the same dimensions. The spacer's one end is closed, while the other end has an open mouth. The plexiglass piece at the top has a cube-like opening of dimensions 0.3 cm x 0.3 cm into the spacer. 0.73 grams of acrylamide, 0.0015 grams of N, N'-methylenebisacrylamide, 0.01 g of potassium persulfate are weighed in a beaker. The crosslinker concentration is reduced as there is no potassium chromate inside the hydrogel. A total of 4.8 ml of water is added to dissolve all the ingredients. The solution is ultrasonicated for 2 minutes. 5 microliters of tetramethylethylenediamine (TEMED), a free-radical initiator, is added to the gel solution. The gel solution is then transferred to the plexiglass mold from the open end. The solution is injected carefully to achieve a 1 cm polyacrylamide gel stripe. After approximately, 24 hours, 1 M $CuCl_2$ is introduced through the open end of the mold. The desired concentration of potassium chromate is inserted through the cube-like opening on the top plexiglas piece. A small drop of oil is added on top of $CuCl_2$ and K_2CrO_4 solution inside the mold to reduce the evaporation of the liquid solutions.

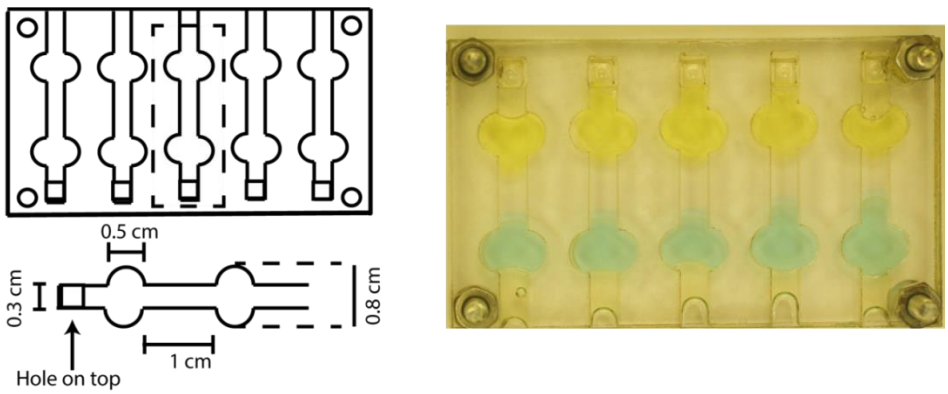

Figure 9: (Left) The dimensions of the mold to prepare a 1 cm x 0.3 x 0.2 cm PAM gel column is shown. The dimensions of each reservoir of electrolytes are 0.5 x 0.8 x 0.2 cm. (Right) Mold with the addition of the copper(II) chloride and potassium chromate reservoirs on each side of 1 cm polyacrylamide gel stripe.

2.4. Determination of Copper(II) chromate's solubility product in water

Copper chromate is synthesized by mixing copper(II) chloride solution with potassium chromate. 6.7 grams of copper(II) chloride and 9.7 grams of potassium chromate are dissolved separately in 250 ml of water each. Both solutions are ultrasonicated till the point a complete dissolution has occurred. Copper(II) chloride solution is added slowly to the potassium chromate solution. The reaction mixture is stirred using a teflon coated magnetic stirring bar for the next 12 hours. Copper(II) chromate is filtered out from the reaction mixture using vacuum filtration. The precipitate is washed with 200 ml of water in 8 subsequent washes. The precipitate is then washed with 200 ml of methanol in 8 subsequent washes. Copper(II) chromate is transferred to a mortar and crushed down fine powder. The precipitates are dried overnight under vacuum at room temperature.

25 mg of Copper(II) chromate is weighed in a glass vial and 2 ml of water is added to it. A total of five samples are prepared for each temperature. The vials are transferred to an oil bath set at desired temperature. The mixtures are stirred using PTF coated magnetic stirring bars for at least 12 hours. After 12 hours, the solution is transferred to a syringe (pre-heated at a higher temperature), and filtered using a syringe filter (pre-heated at higher temperature). 0.5 ml of the filtrate is diluted to 10 ml solution with water, to prevent any dissolution. 2 ml of this solution is further diluted to 10 ml with water. The solutions are then analyzed with UV-Vis spectroscopy between 365 - 370 nm to obtain the concentration of chromate ions. A calibration plot for UV-Vis spectroscopy is obtained from 0.01, 0.025, 0.05, 0.075, 0.1 and 0.25 mM solutions of potassium chromate prepared by appropriate dilutions. The concentration of chromate ions is determined using Beer Lambert law.

2.5. Device for Controlling Temperature

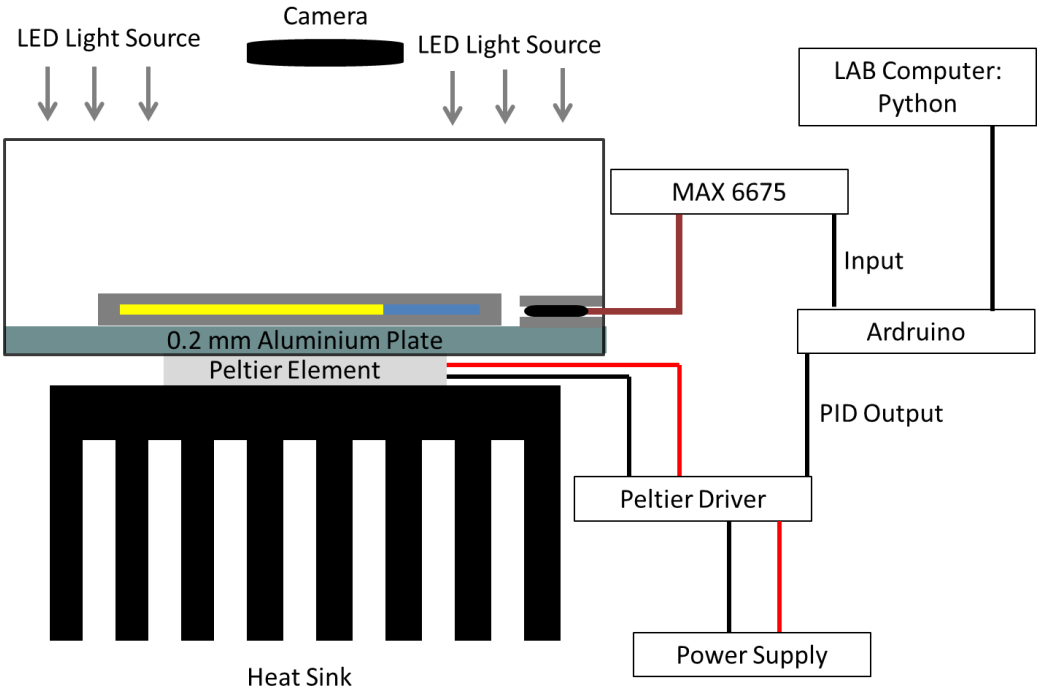

Figure 10: The experimental setup for controlled temperature experiments.

The temperature is controlled by a home-built setup using a Peltier element. Peltier element works under the principles of thermoelectric cooling and the effect is known as the Peltier effect. The Peltier element employed in our device is TEC1-12706. TEC1-12706 has a maximum current rating of 6.4 Amps, a maximum voltage rating of 14.4 volts. The two sides of the Peltier element are coated with locally obtained, silicon-based thermal paste and is sandwiched between a heat sink and a 2 mm thick aluminum plate. Thermocouple is sandwiched between two plexiglass plates in a similar fashion as hydrogels. We use a K-type thermocouple with temperature ratings between -20 to 80-degree Celsius and interface it with an Arduino Nano, using MAX-6675 which digitalizes the signal from the thermocouple. MAX-6675 provides a 12-bit resolution to the temperature data, i.e. 0.25 degree-celsius. Arduino Nano is in interface with Spyder Python in a desktop computer. Data from MAX-6675 is the input to the PID loop. PID output drives the Peltier Element using a Peltier Driver through Arduino Nano. Peltier

Driver used in our setup is a half-bridge, BTS 7960B DC Motor driver. The BTS 7960B DC Motor driver has a maximum current rating of 40 Amps and working voltages range from 5.5 to 27.5 Volts.

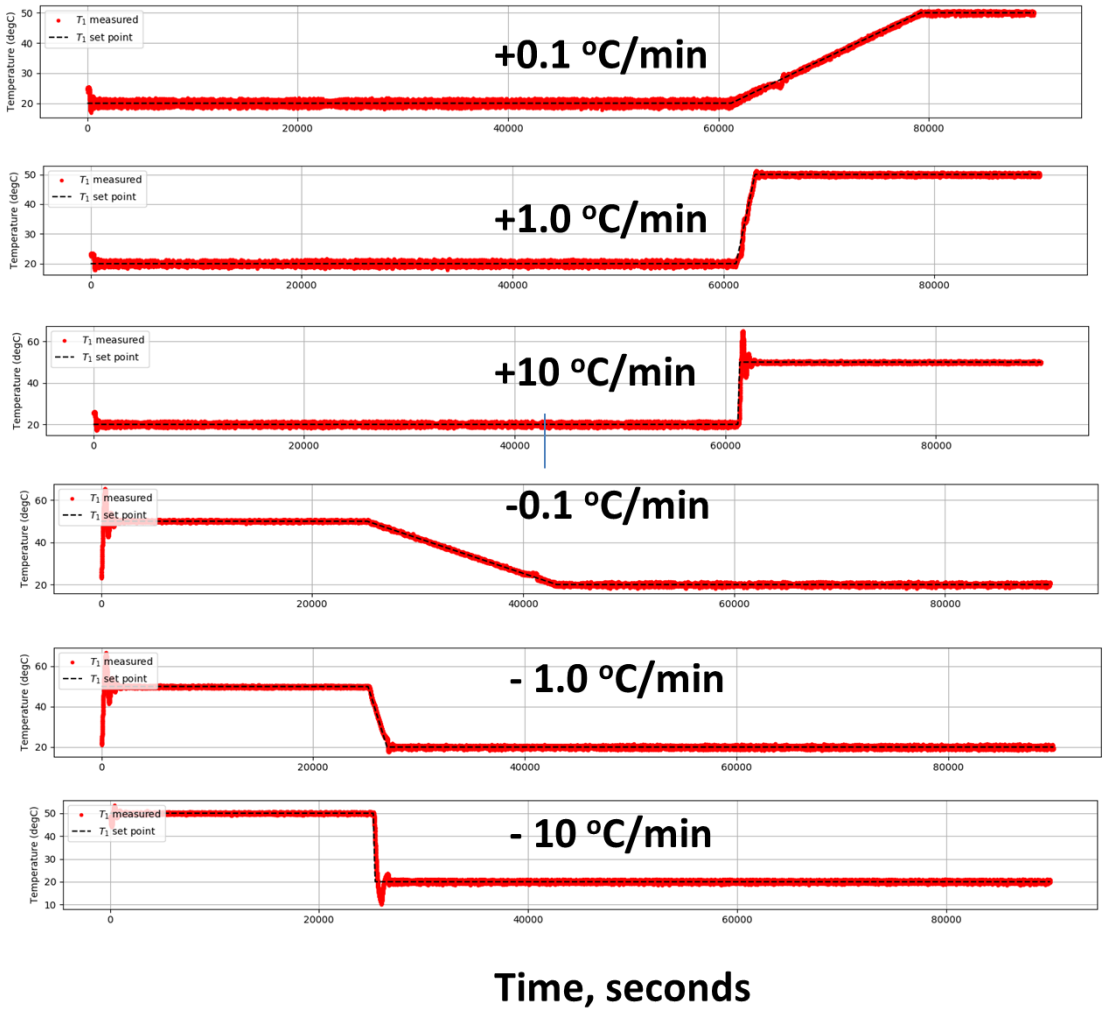

Figure 11: The home-built device can keep the temperature constant over time and then ramp the temperature at the desired rate to a certain temperature. Here the first three plots show the temperature is increased from 20 to 50^{o}C at 0.1, 1, and 10^{o}C/min, respectively. The last three graphs show a decrease from 20 to 50^{o}C at 0.1, 1, and 10^{o}C/min, respectively.

2.6. Imaging and Analysis

2.6.1. Determination of spacing coefficient

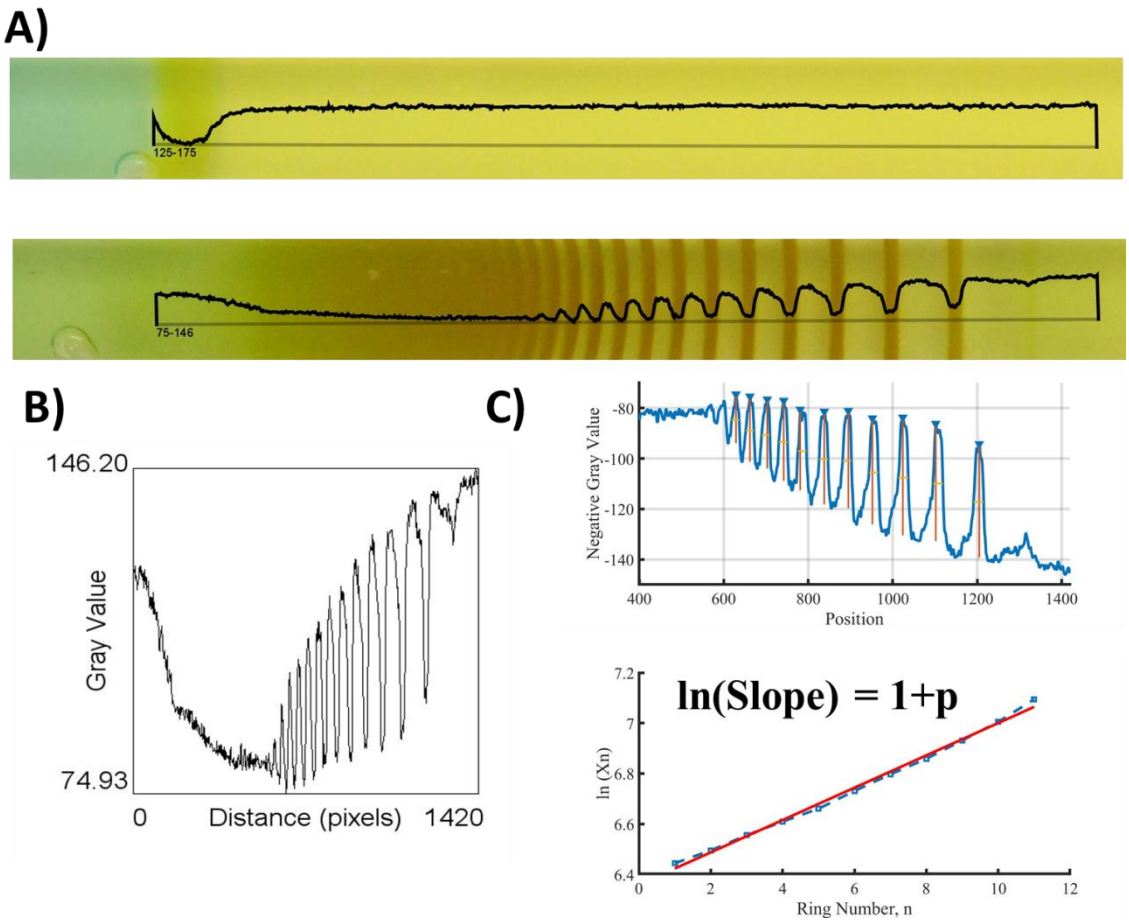

Figure 12: A) The gray value profile (black line) is plotted for the first photo (top, 0 hrs) and the last photo (bottom, 24 hrs) taken during the experiments. The rings are appearing as dips in the gray-value. B) The gray-value plot over the distance in pixels. C) The negative of the gray-value is plotted against distance, i.e., position in Matlab. The rings now appear as peaks and using a built-in functionality of Matlab, i.e., 'Findpeak', the position of a ring can be obtained. The logarithm of position is plotted against the ring number and the slope gives us 1+p (the spacing coefficient).

Liesegang Rings are quantified by extracting the information about the position of the rings using ImageJ software. Image of LPs is loaded to ImageJ and the 'gray-value' of a

single-line selection is plotted. Gray-Value refers to a combination of the three-color components of the image i.e. red, green, and blue. The formula used for quantifying the gray value is 0.299red + 0.587green + 0.114blue. Gray value plot shows the rings as the sharp dips in the gray value. Following that, the raw data of the gray value vs pixel position plot is loaded into Matlab. The negative of the gray value is plotted so that rings appear as peaks. Position, width, and prominence are determined by a built-in functionality of Matlab i.e. 'Findpeaks'. The position of the ring (X_n) is determined for each peak, by finding the distance at which local maxima in negative gray value occurred. 'Prominence' is the maximum gray value. Width is determined by full-width at half maxima. The spacing law is determined by taking a logarithm of positions then plotting the graph of ln(Xn) versus the number of rings. The slope of this plot is the spacing coefficient.

2.6.2. Determining Time Law

The time law is determined by loading the stack of images into ImageJ. Each frame in the image stack represents an image taken at a 5 min interval. The point of contact (PC) between the gel and the outer electrolyte is chosen as a reference point for all the images. The position of the rings is determined by streching the line from PC to the middle of the ring. The time is decided as the point where ring starts to form. A plot is plotted regarding the relationship between the postion of the ring and the square root of time.

2.6.3. Image processing for tracking diffusion of Copper ions

The diffusion of copper ions is qualitatively tracked by converting the images from RGB to HSB stack in OpenCV (figure 13). Following that, a mask is applied for HSV values of [28, 0, 0]. HUE values above 28 are masked by the color filter. The resulting image is converted to a binary image of 0 and 1, where 0 illustrates HUE values below 28 and 1 all the HUE values above 28. In the final image, copper ions are represented as white, and black refers to the polyacrylamide gel matrix without any inner electrolyte. In this way, the signal to noise ratio for tracking the diffusion of copper ions is improved.

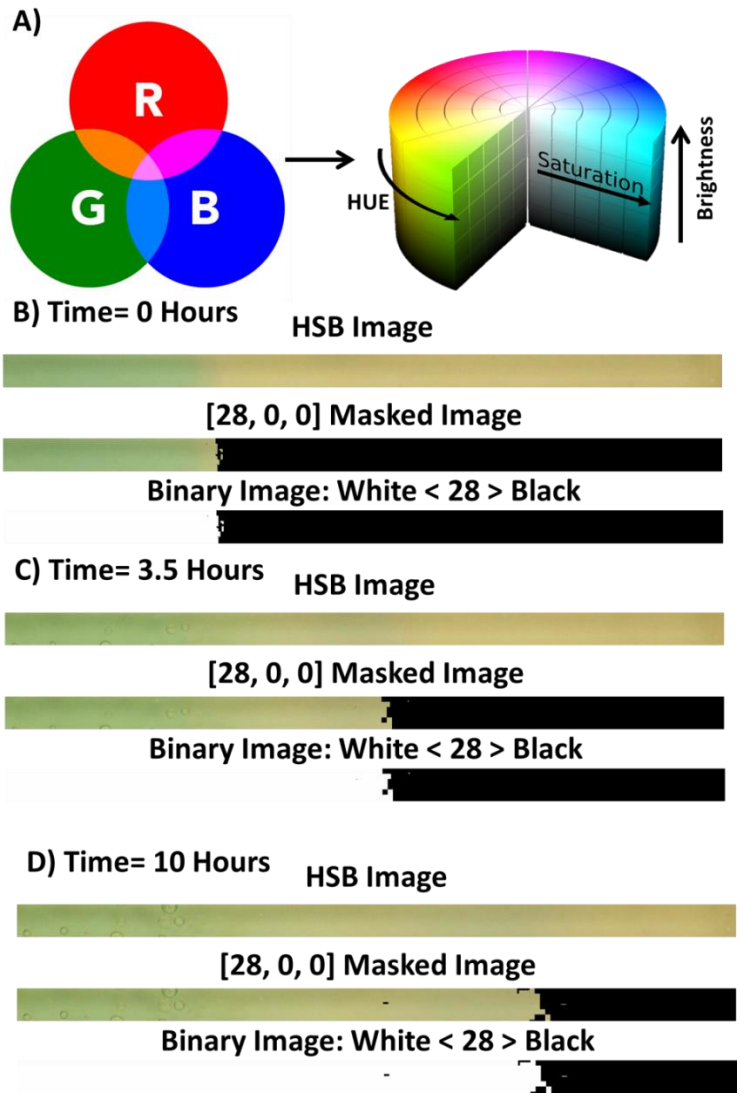

Figure 13: A) The difference between the understanding of RGB and HSB is illustrated. Images are converted from RGB to HSB. B), C), D), The images from the diffusion of copper chloride in PAM (without any inner electrolyte) at different times, 0 hours, 3.5 hours and 10 hours. A specific filter for HUE value of 28 is chosen without any regard to saturation and brightness. Following, a mask is applied with respect to that filter. Finally, the images are converted to a binary image with white representing copper ions, and black referring to PAM (without any inner electrolyte).

2.7. Sample Preparation for SEM Analysis

The size distribution of patterns is analyzed using SEM. Hydrogel sample with freshly formed periodic precipitates at a desired temperature is placed horizontally in a glass flask. The flask is vacuumed and transferred to liquid nitrogen bath for the next 30 minutes. Frozen hydrogels are placed on a stand pre-cooled with liquid nitrogen. The samples are cut in half using a steel blade and transferred to a petri dish, with the freshly cut side on top. Petri dish is covered with aluminum foil and then placed under vacuum at room temperature for 24 hours.

Scanning Electron Microscopy (SEM) and Energy Dispersive X-Ray (EDX) Analyses.

The surface morphology of gel samples were imaged and analyzed with a Quanta 200F model SEM with an accelerating voltage of 10 kV. Samples were coated with Au-Pd. The size of the particles was determined using digital image analysis ImageJ software (figure 14).

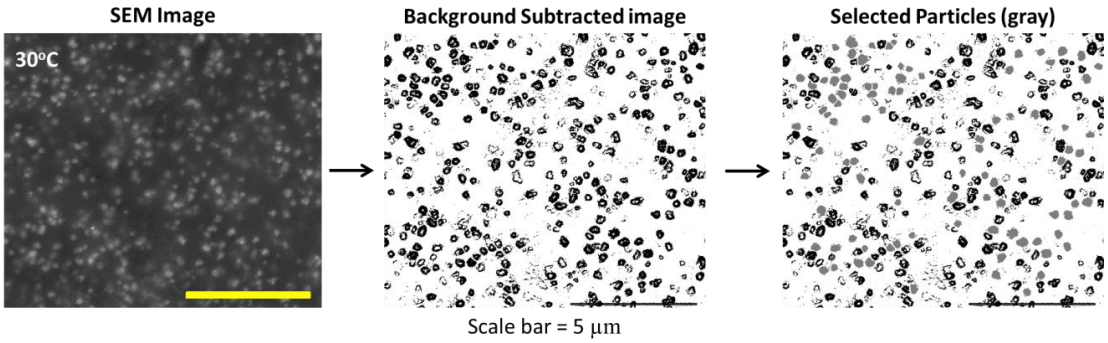

Figure 14: Image processing applied to an SEM image. Particles appear as bright spots in the image. Background subtraction is performed in ImageJ to obtain particles as black dots with white background. Particles (grey colored) are selected per image for size determination. 3 photos are analyzed for each ring and a total of 100 particles is considered for sampling.

Chapter 3

3. Results and Discussion:

3.1. Emergence of Liesegang patterns at different temperatures

In our system, Cu^{2+} ions diffuse into the gel from one side (1D) and react with CrO_4^{2-} ions homogeneously distributed inside the gel.

$$A + B \rightarrow C \text{ (Colloids)}$$

$$C \rightarrow P$$

In the Liesegang phenomenon, temperature affects the diffusion of Cu^{2+} ions, the rate of colloid formation, and stability of the colloids to form periodic precipitates. Therefore, pattern evolution is expected to be visually distinctive concerning the different temperatures. LPs are allowed to form, at a constant temperature, for 24 hours (Figure 15A). Periodic patterns are observed in the range from 20 to 60^oC. With every 10^oC increments in increasing temperature, wider depletion zones between periodic precipitates occur. The position of the last band is further in the spatial coordinate for every 10^oC increment. Figure 15B also illustrates how the relationship between point of contact (PC) and precipitation begins (PB) varies with increments in temperatures. The distance between PC and PB decreases at a higher temperature as compared to lower temperatures.

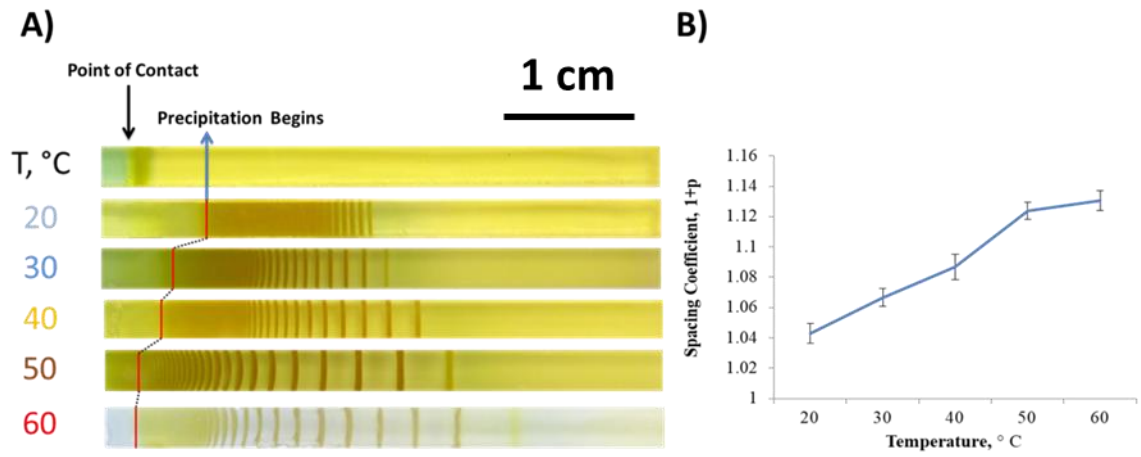

Figure 15: A) Liesegang Patterns formed at 20, 30, 40, 50, and 60^{o}C. PC indicates the point of contact between the polyacrylamide gel surface containing 0.01 M K_2CrO_4 and 1 M $CuCl_2$ solution. PB indicates the point at which the precipitation of $CuCrO_4$ begins. Scale bar is 1 cm. B) The variation of spacing coefficient in each of the samples at different temperatures.

Furthermore, the visually distinctive features like wider depletion zones and the position of the last ring are mathematically quantified by the spacing coefficient. Spacing law is one of the benchmark characterizations of LPs.

The spacing law is:

$$\mathbf{1} + \boldsymbol{p} = \frac{\boldsymbol{Xn} + \mathbf{1}}{\boldsymbol{Xn}}$$

where X_n and X_{n+1} are the positions of the nth and (n + 1) the bands measured from the gel surface, respectively, and p is the so-called spacing coefficient. PC is chosen as a reference point for all the samples. Figure 15B illustrates how the spacing coefficient demonstrates a direct relationship with temperature.

Figure 16 shows the shifts in distance between PC and PB over time. At the start of diffusion, continuous precipitation is observed. This precipitation zone re-dissolves and seemingly, the precipitation front propagates. For instance, at 20^{o}C dissolution occurs in

various instances until 12 hours, resulting in a higher distance between PC and PB. At 30 and 40^{o}C, stabilized precipitation begins (SPB) after 6 hours, i.e. no significant dissolution occurs later on. Following the trend, SPB occurs after 2 hours into the reaction-diffusion processes at 50 and 60^{o}C. Thus, the distance between PC and PB evolves and PB stabilizes both closest to PC and earlier in time coordinate at 60^{o}C compared to lower temperatures. This dissolution of $CuCrO_4$ can be related to several factors. And such dissolution is not unique to this system. Similar behavior occurs in the $Co(OH)_2$ [37] system in which periodic precipitates dissolute. This observation occurs as a result of complexation reactions. Since the dissolution is limited to the beginning of continuous precipitation, our results may find their explanation in the dissolution of small colloids. For the precipitates to be stable in the gel media, they need to aggregate into bigger particles. Colloid diffusion is limited in gel media as a result smaller colloids dissolute and re-precipitates to form bigger aggregates. Thus, the occurrence of earlier SPB and lower distance between PC and PB at higher temperatures could lead us to conclude one of the following: 1) aggregation of $CuCrO_4$ colloids could be favored by higher temperatures (higher k_bT i.e. an increased energy possessed by the particles for aggregation at higher temperatures), 2) naturally, the particle size of $CuCrO_4$ colloids could increase with temperature [38]. Each of these factors is interrelated since precipitation threshold is a measure of the number of colloids and their sizes at a specific position in the media. The exact conclusion is far from reach, however, visually distinctive features (PC, PB, and SPB) point towards an essential interplay between different factors.

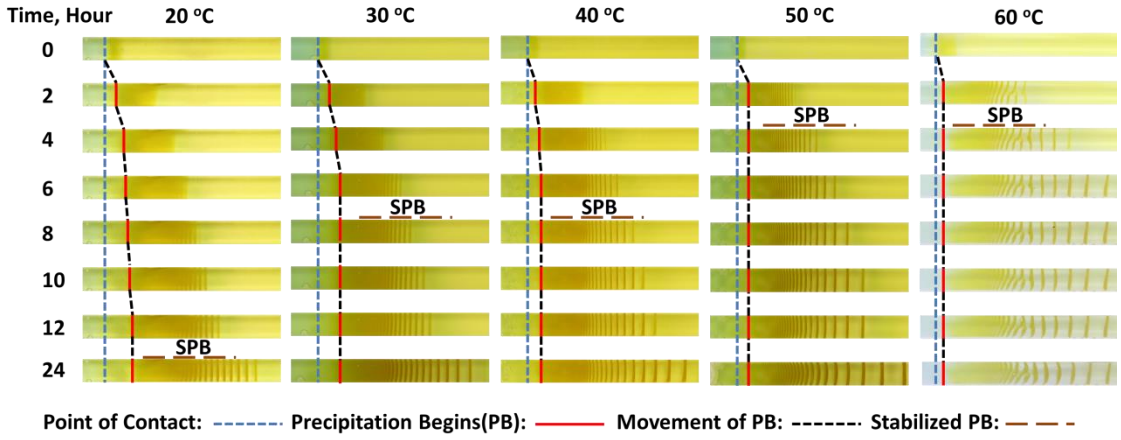

Figure 16: Spatial and time evolution of PB for different temperatures. SPB indicates the time at which PB stabilizes at a certain point. The distance between point of contact (PC) and PB is reducing as the temperature is increased.

The space-time relationship is demonstrated in figure 17. The slope of the graph increases according to the increments in temperature. LPs form further in the spatial coordinate at a faster rate at higher temperatures.

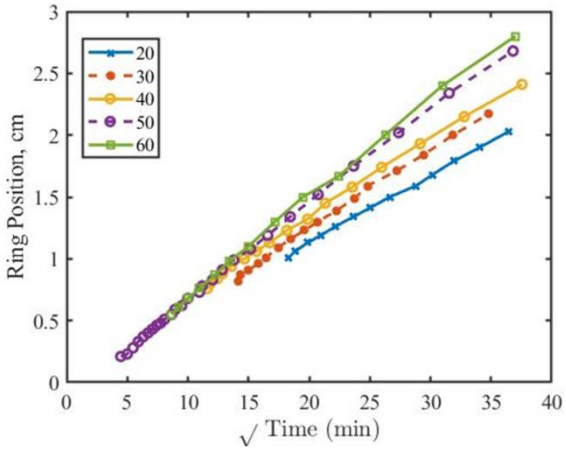

Figure 17: The variance between the time and position of the evolution of the patterns is demonstrated.

3.2. SEM analysis of LPs forming at a specific temperature

The occurrence of late SPB at lower temperatures (figure 16) was reasoned by the hypothesis of very small particle size in the beginning of the reaction-diffusion. Here, we demonstrate the effect of temperature on the particle size in Liesegang phenomenon. LPs appear as bands of concurrent periodic precipitates; these bands result from the aggregation of small particles. Figure 18 illustrates the difference between a depletion zone i.e. no ring region and ring region at resolution of 5 micro meters. The ring region of the gel consists of particles as bright spots and EDX spectrum confirms the presence of copper(II) chromate particles by the occurrence of chromium peak in ring region only.

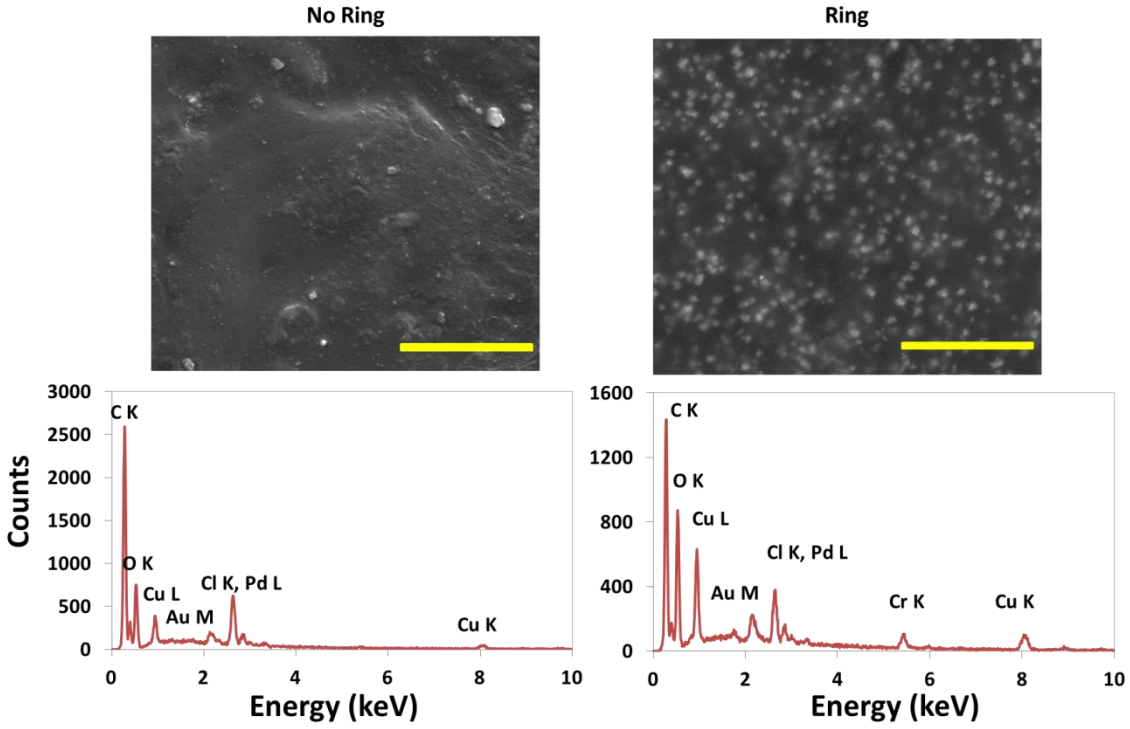

Figure 18: SEM images showing the difference between a depletion zone (no ring) and ring region. The scale bar (yellow line) represents 5 µm. The elemental analysis using EDX shows difference between ring and no ring region, with the presence of Cr peak in the ring region only.

Samples from each constant temperature experiments were analyzed under SEM for determination of particle sizes. Here we show the relationship between temperature and particle size in Ring 1, 5, 7 and 9 (the Last Band). In figure 19A, SEM images of ring 1 and 5 from constant temperature experiments are shown, along with, the histograms showing the distribution of particle size. Figure 20A compares the SEM images of ring 7 and 9, forming at different temperatures, along with, the histograms showing the distribution of particle sizes. The general trend observed is an increase in the particle size along the ring number as reported in literature [39]. However, the particle size for a simultaneous ring varies a lot with temperature. Particles at ring 1 from the sample kept at 60^{o}C, has considerably higher size then particles observed for ring 1 from sample kept at 20^{o}C. Similarly, every 10^{o}C increment in temperature increases the particle size for the simultaneous ring. The particle size and distribution at different temperatures are visually very distinct from each other at ring 1, 5, 7 and 9. The visual observation is further strengthened from the particle size histograms.

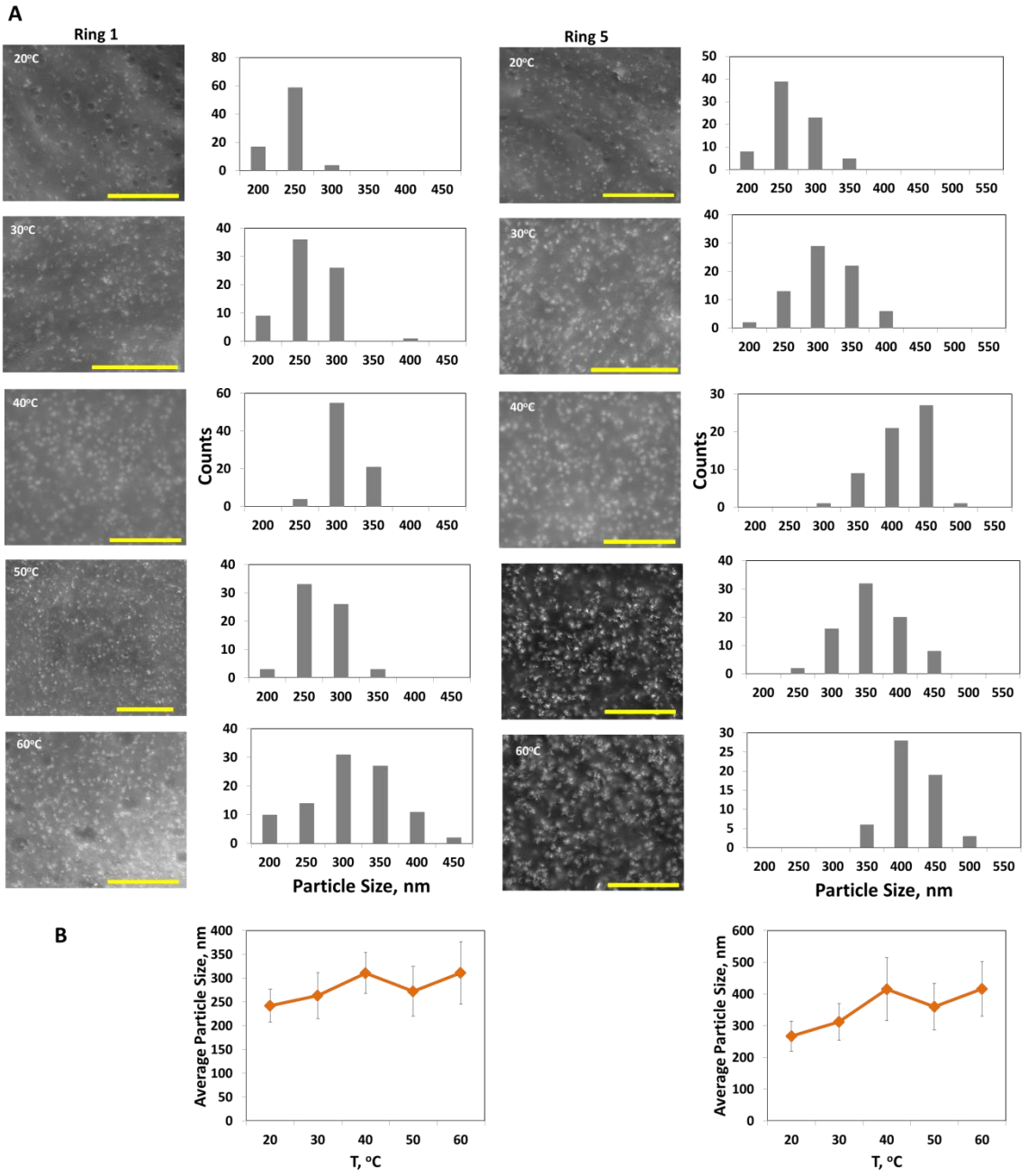

Figure 19: (A)SEM images of ring 1 and 5 from samples at different temperatures. The histograms in front of the SEM images show the distribution of particle size. The scale bar (yellow line) represents 5 µm. (B) Average particle size in Ring 1 and 5 at different temperatures.

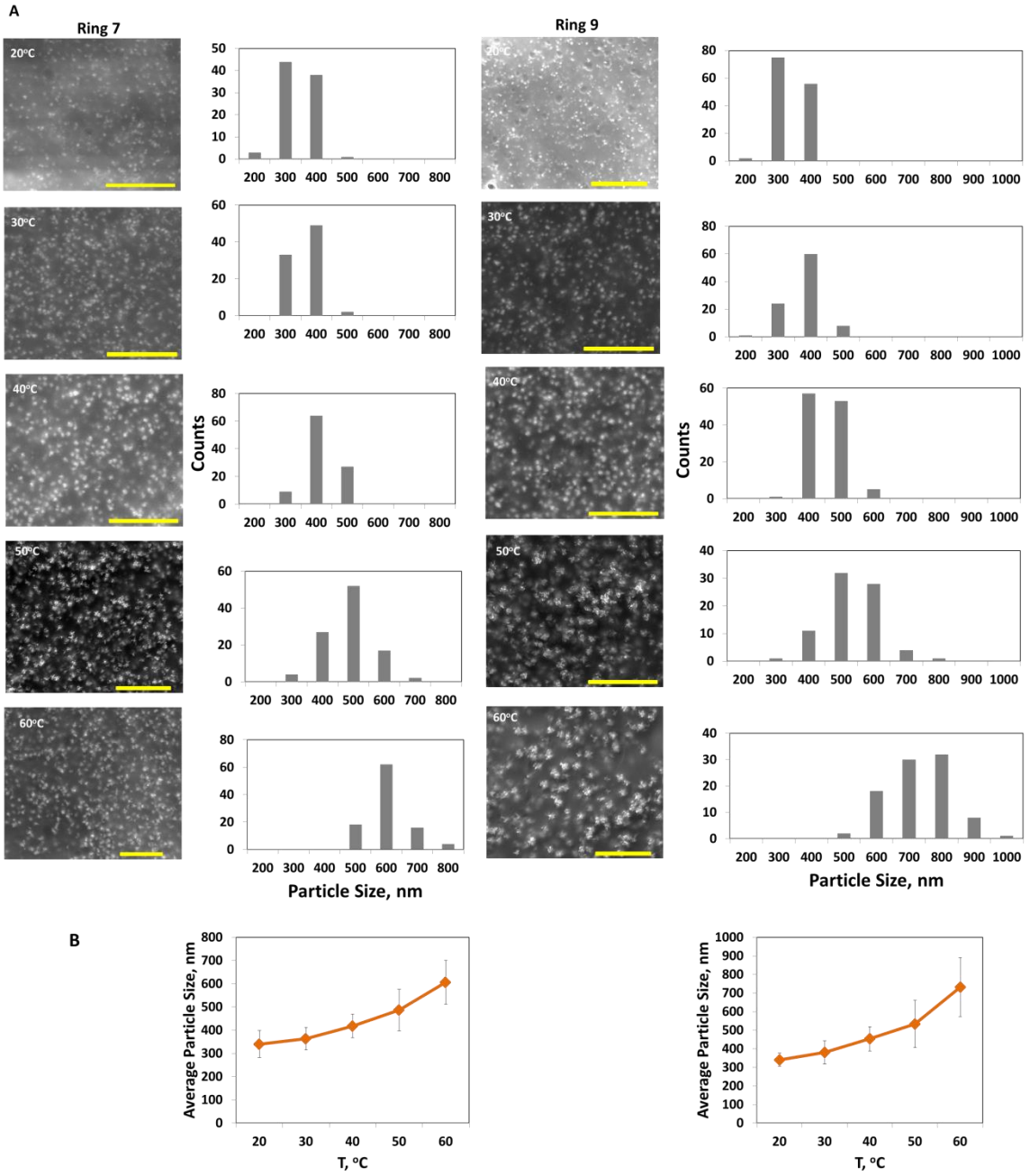

Figure 20: SEM images of ring 7 and 9 from samples at different temperatures. The histograms in front of the SEM images show the distribution of particle size. The scale bar (yellow line) represents 5 µm. (B) Average particle size in Ring 7 and 9 at different temperatures.

3.3. Understanding the Factors at play

Diffusion Coefficient (k_d) of copper ions in polyacrylamide gel, Precipitation Threshold (i.e. the number/ concentration of colloids required for a band to occur) and Reaction Coefficient (k_p) of the reaction between copper ions and chromate ions are independently affected by temperature. Precipitation threshold is directly affected by the solubility of the copper(II) chromate, therefore, the solubility product (K_{sp}) of copper(II) chromate at different temperatures is to be determined. For a reaction-diffusion system, k_d, k_p, and K_{sp} are interlinked with each other, thus in order to quantify effect of temperature on LPs each of these need to be treated independently in most similar fashion to our system.

3.3.1. Understanding the Diffusion

The diffusion coefficient in porous media like hydrogels is related to the porosity of the media. And to discover the relationship between diffusion coefficient and temperature, the link between the porosity of polyacrylamide hydrogel and temperature needs to be uncovered. Since copper ions can complex with the polyacrylamide matrix, the ability of copper ions to diffuse can also vary with temperature. The complexing ability of copper ions might also alter the porosity of the hydrogel. This claim finds its basis in the work of Korevaar et al, where they demonstrate that diffusing fronts can result in the appearance of a physical wave [40]. Therefore, we understand this problem by preparing polyacrylamide hydrogels, without any inner electrolyte (Potassium Chromate) and introduce a reservoir of copper ions from one end (1D). The diffusion of copper ions is monitored for 12 hours at a constant temperature.

Figure 21 shows how the copper front diffuses inside the hydrogels at different temperatures. Color filtering is applied (see Section 2.7.3 for further details of image processing) to understand the position of the copper front inside the hydrogel more precisely. As illustrated in figure 21, the Cu^{2+} front moves faster and further at higher temperatures.

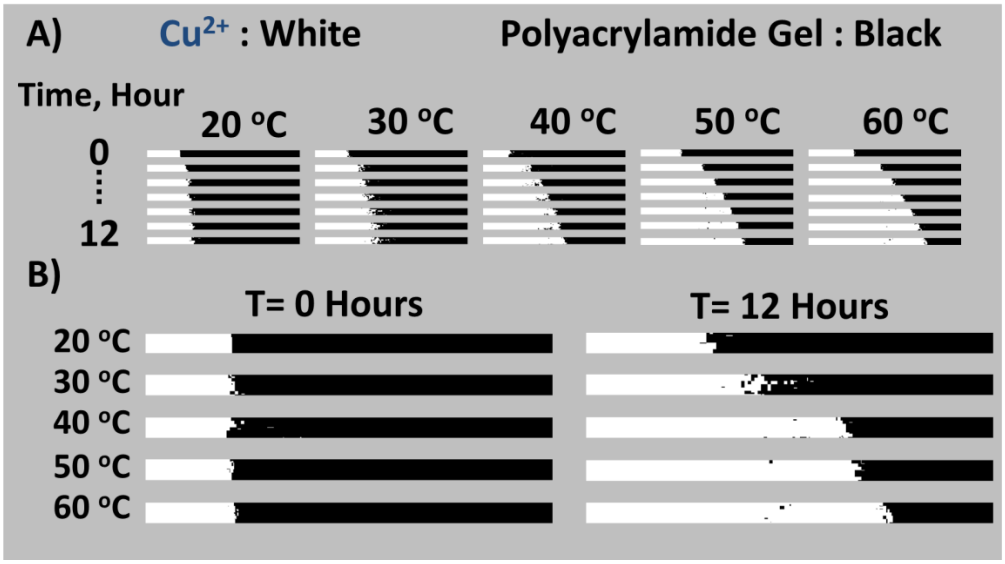

Figure 21: Diffusion of copper ions in polyacrylamide hydrogel without any inner electrolyte is monitored at different temperatures. The presence of diffusing copper ions are represented in white. A) Diffusion of copper ions at each temperature from 0 to 12 hours with time interval between each frame of 2 hours. B) Comparison of how the diffusion in a constant time interval differs with each temperature. T=0 hours, the first frame, and T= 12 hours, the last frame of the time lapse for each of the temperatures.

3.3.2. Understanding the precipitation threshold

Conventional Liesegang phenomenon is observed for ions producing sparingly soluble salts in aqueous media. Periodic bands of the salt arise inside hydrogels when colloids aggregate to form bigger particles. This process occurs when the concentration of colloids at a certain point (band location) surpasses the precipitation threshold. Solubility product plays an important role in determination of a precipitation threshold for the system. The indirect relationship between the precipitation threshold and the solubility product indicates that for salts with high K_{sp} will require a higher concentration or bigger size of colloids to aggregate and vice versa. This relationship also alters the spacing between the bands. As a reaction-diffusion system propagates, the concentration of inner electrolyte depletes behind and in front of the band. For the next band to occur the outer electrolyte diffuses further and the concentration of colloids rise to form the next band,

however this time at a different place in hydrogel [37]. Now if we have two sparingly soluble salts, one with the K_{sp} value higher than the other. The creation of the second band will require higher concentration of the colloids for the salt with higher K_{sp}. Thus, the colloids will be forming and dissolving to form bigger particles and aggregate further in the spatial coordinate to form the next consecutive band. As a result, spacing between patterns formed for the salt with higher K_{sp} will be greater in comparison to the system having lower K_{sp}. Solubility product also affects the particle size. For salts with lower K_{sp} values, the supersaturation is high, and colloids surpass precipitation threshold easily. Hence, dissolution of colloids to form bigger aggregates occurs at a lower frequency than for the salt with higher K_{sp}. Thus, solubility product holds an essential place in the equation, from existence of bands, to the spacing between them to the size of the aggregates.

In our system, LPs of copper(II) chromate are forming at different temperatures and solubility product is varying with temperature. In order to determine the solubility product at the different temperatures used in the experiments, copper(II) chromate is separately formed from its aqueous ions and the solubility product is determined in a similar fashion as Coetzee et al. reported [41]. (The experimental details of this procedure are given in Section 2.4). Here in figure 22 we illustrate how the solubility product changes with temperature. The dissolution of copper(II) chromate is assumed to occur as,

$$CuCrO_{4\,(s)} \rightleftharpoons Cu^{2+}{}_{(aq)} + CrO_4{}^{2-}{}_{(aq)}$$

Solubility product of copper(II) chromate rises with the temperature of the system (figure 22D). Maximum absorption between 365-370 nm [42] is used for the calculation of concentration of chromate ions using the molar absorption coefficient, 4.048 $L \cdot mol^{-1} \cdot cm^{-1}$ (figure 22B). Our results about the increase in the spacing between the rings (figure 14), occurrence of earlier stabilized precipitation (figure 16) and an increase in the size of the particles (figure 19 and 20) can be explained by dramatic increase in the values of the solubility product as the temperature of the system rises.

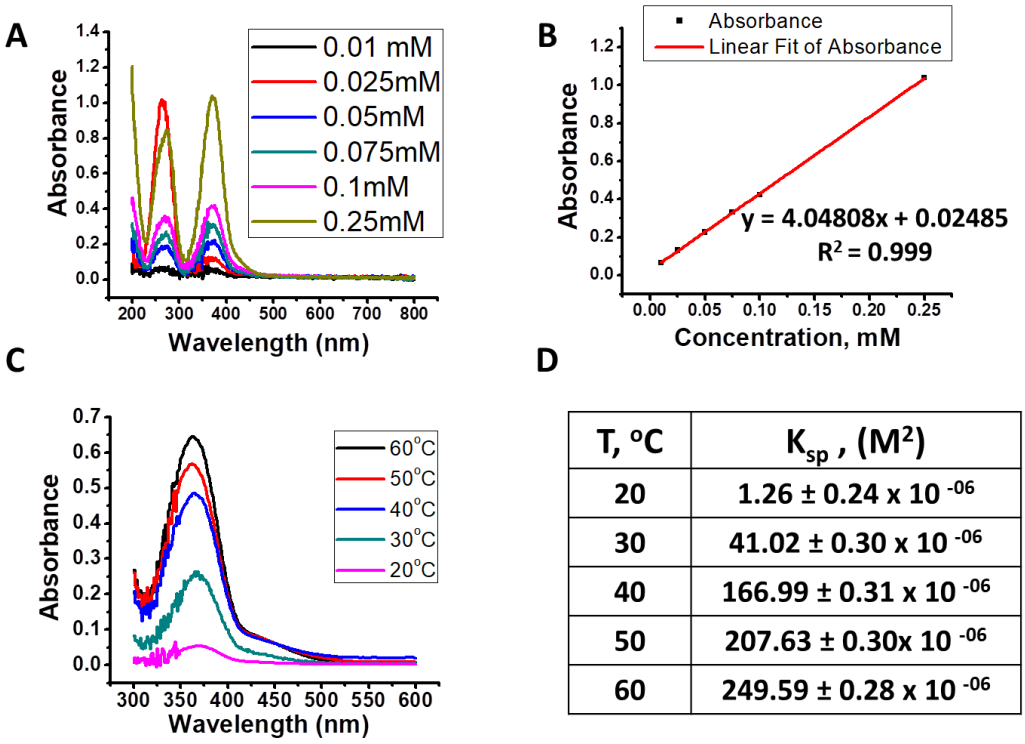

T, °C	K_{sp} , (M^2)
20	1.26 ± 0.24 x 10 $^{-06}$
30	41.02 ± 0.30 x 10 $^{-06}$
40	166.99 ± 0.31 x 10 $^{-06}$
50	207.63 ± 0.30x 10 $^{-06}$
60	249.59 ± 0.28 x 10 $^{-06}$

Figure 22: (A) UV-Vis absorption spectra of 0.01, 0.025, 0.05, 0.075, 0.1 and 0.25 mM. of potassium chromate solutions. (B) Calibration plot for determining the concentration of chromate ions, plotted from the data obtained in (A) at 365-370 nm. (C) UV-Vis absorption spectra of samples from copper chromate solutions at different temperatures. See section 2.4 for the details of the experimental procedure. (D) The variance in solubility product as a function of temperature is shown in table. The error bars are calculated from (A) and (B) independent experiments.

3.3.3. Understanding the Reaction Coefficient

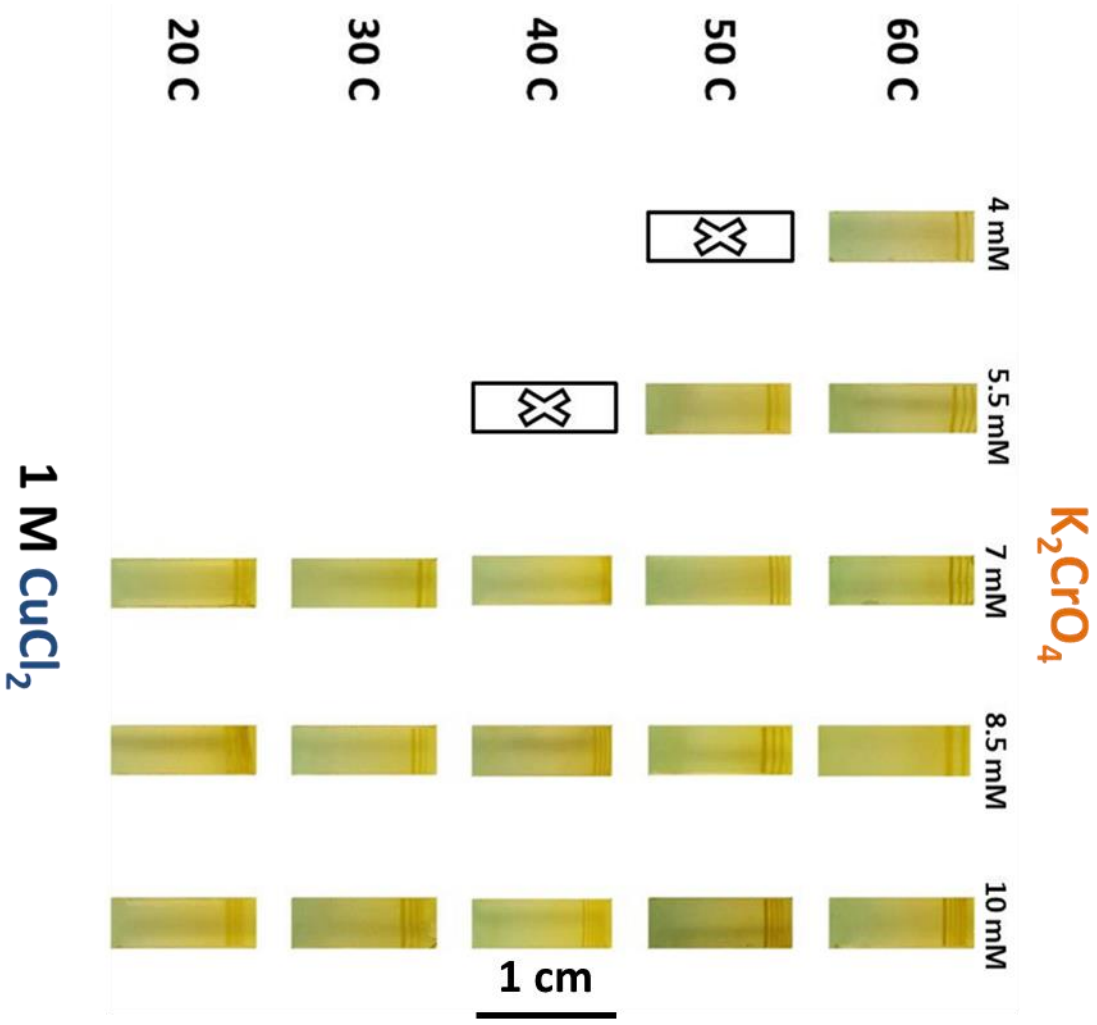

Figure 23: The occurrence of the precipitation band in counter diffusion experiments (see section 2.3 for mold preparation). The concentration of K_2CrO_4 is varied from 4 mM to 10 mM. K_2CrO_4 is allowed to diffuse against 1 M $CuCl_2$, at temperatures from 20 to 60^{o}C. Scale bar is 1 cm.

Here in figure 23, we prepare a 1 cm polyacrylamide gel matrix without any inner electrolyte (See Section 2.3 for details on experimental preparation), and introduce a reservoir of Cu^{2+} ions from one end and another reservoir of potassium chromate form the other end. The two reactants are allowed to simultaneously diffuse into the hydrogels and finally react with each other to produce a precipitation band. This is followed by the formation of the revert periodic precipitation patterns. The concentration of potassium chromate is varied between 4 mM and 10 mM and the concentration of copper chloride is kept constant at 1 M (See Section 2.3 for experimental details).

The trend indicates that with increasing temperature, the precipitation threshold decreases (see section 3.3.2 for discussion). The results in figure 23 do not demonstrate a decrease in the solubility product with increasing temperature. The occurrences of a precipitation band for lower concentrations of chromate at higher temperatures can be due to aggregation of large particles (as particle size increases with the temperature of the system, see figure 19 and 20).

The feature extracted from the counter diffusion experiment is the time it takes for the band to appear after the two fronts have met (figure 24A). Figure 24B to F illustrates the time required for the bands to appear for different concentrations of potassium chromate. The results indicate for each temperature value, less time is required for a band to appear at higher concentrations. The relationship between time for the formation of the precipitation band and the temperature for a particular concentration is plotted in figure G. These results indicate that from the time the fronts meet to the point a precipitation band is formed; with increasing temperature, all processes occur at an increased rate; 1) the rate of formation of colloids, their dissolution and reformation, 2) surpassing the precipitation threshold, 3) aggregation of colloids into the bands. Therefore, we can conclude that the reaction rate is being positively affected by the increase in temperature.

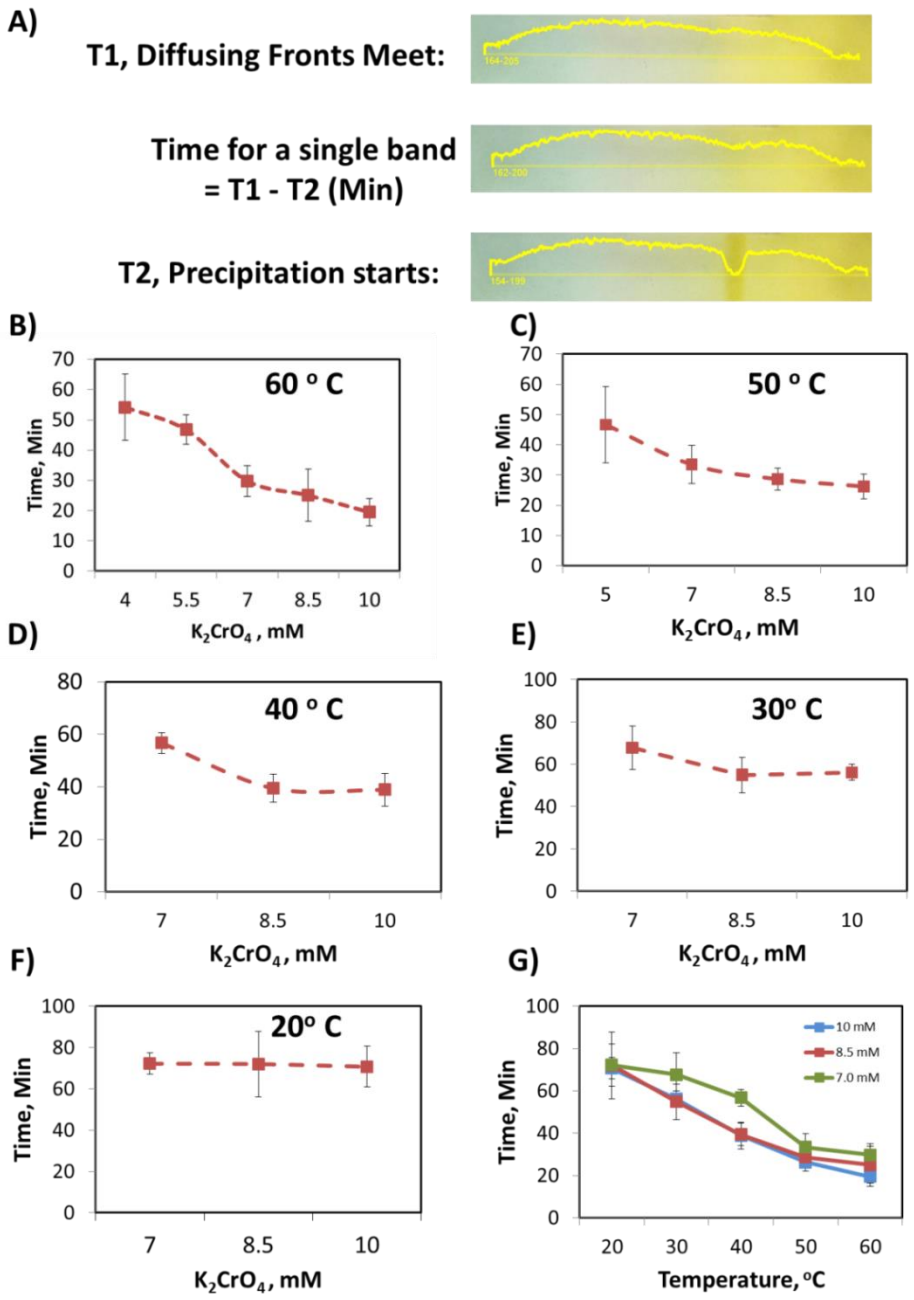

Figure 24: A) The time at which the fronts meet is denoted as T1, and the time for the precipitation band to appear visually is demonstrated as T2. The time for formation of the single precipitation band is the difference between T2 - T1. Plots B to F indicate the time for the formation of a single precipitation band at different potassium chromate concentrations, from 60 to 20^{o}C, respectively. Plot G shows the links the time for the appearance of the band versus temperature at a particular concentration.

3.4. Reaction-Diffusion Pushed and Pulled

3.4.1. Pulsing the System at different times- The effect of the time of the temperature change on the LP

Due to the non-equilibrium dynamics in nature, patterns in nature do not necessarily exhibit simple decreasing or increasing trends. So far, our experiments demonstrate that the pattern evolution differs for each temperature value of the system. They display, temperature has a considerably high impact on the pattern formation and the complex triangle between reaction coefficient, precipitation threshold, and, diffusion coefficient alter periodic precipitation at different temperatures. So far, it has been concluded that temperature certainly alters the time law and the spacing law in LPs. In this section, we alter the temperature as the LP formation proceeds and try to determine the effect of this change on the diffusion, reaction rate, and the solubility, all of which appear as a sum in the alteration of the LPs formed.

The initial experiment is to understand how LPs evolve when subjected to considerable temperature change at a specific time during the LP formation. For this reason, LPs are allowed to form at 60^{o}C and after a certain time, the temperature of the system is lowered to 20^{o}C. At this stage, the samples are allowed to cool down to 20^{o}C on bench-top. Similar surroundings ensure that the temperature variation between different samples is considerably low. In this experiment, LPs are allowed to form at 60^{o}C for 2 hours, 4 hours, 8 hours, 10 hours, and 12 hours, followed by a subsequent decrease in the temperature to 20^{o}C.

Figure 25A shows the visual difference between the patterns evolving through different temperature profiles. As expected, the spatial distance covered by the periodic precipitates increases over time at higher temperatures. The blue arrow (figure 25A) indicates the last ring formed at 60^{o}C. The unprecedented visual feature that arises in LPs is the occurrence of the wide depletion zone after temperature is lowered. A wide depletion zone starts to form between the last pattern formed at 60^{o}C and the first post-

transition pattern, upon transitioning from 60 to 20°C. Following this first post-transition pattern, the spacing coefficient, 1 + p, shows a sudden increase due to the wide depletion zone (Figure 25B) and then 1+p starts to decreases. Similarly, the widths of the patterns demonstrate a decreasing trend upon the decrease in the temperature, figure 25C. The time at which the patterns are transitioned to 20°C plays a crucial role in the number of patterns formed before and after the transition. Moving from earlier to later transition times, the number of post-transition patterns decreases.

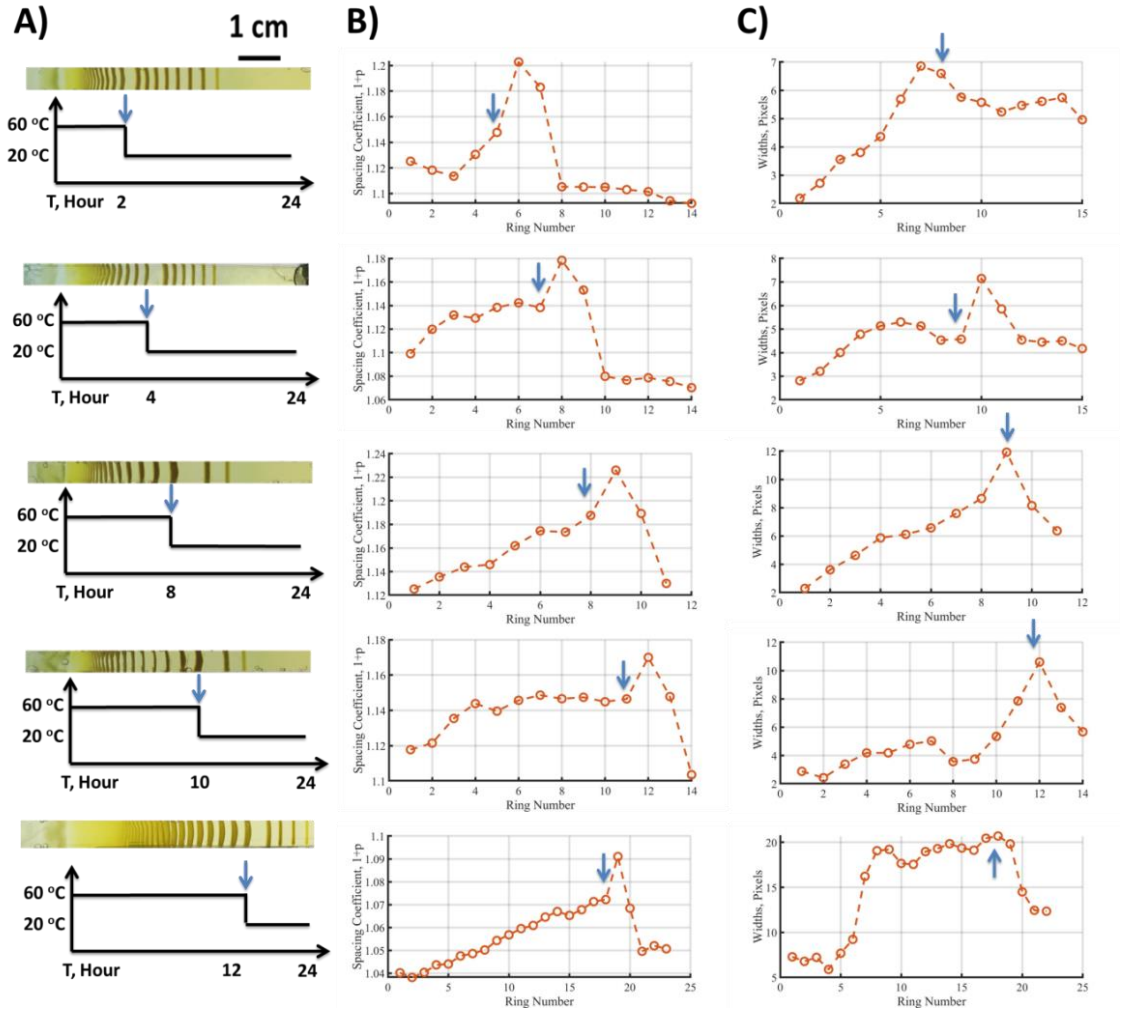

Figure 25: Pattern forming system with different transition times of temperature decrease. (A)From top to bottom, the samples are kept for 2 hours, 4 hours, 8 hours, 10 hours and 12 hours at 60°C during the LP formation, then transferred to 20°C till the 24th hour. Scale bar is 1 cm. (B) The variation in the spacing coefficient of the patterns for different transition times. (C) The variation in the widths of the patterns. The blue arrow marks the point of transition.

3.4.2. Pulsing the System with different 'force' values – The effect of the magnitude of temperature change on the LP

Different time transition experiments (Section 3.4.1) provided us some trends in the spacing coefficient and widths of the patterns as we change the temperature. In this section, we aim to see if the extent of a temperature difference between the initial and final temperature has any effect on the pattern formation. In figure 26, we have two sets of experiments: 'cooling down' and 'heating up'. In the case of cooling down, the rate of cooling is with the same as the different time transition experiments. In the case of heating up, the samples are transitioned to an oil-bath pre-heated to the desired final temperature. The samples are placed at initial temperatures ranging from 30 to 60^{o}C in figure 26A. The time of transition is fixed at 6 hours to achieve a considerable number of periodic precipitation patterns in both pre and post-transition periods. After 6 hours, the samples are cooled down to 20^{o}C creating temperature differences of -10, -20, -30, and -40^{o}C. Accordingly, the spacing coefficient of patterns before and after the transition is plotted in figure 26B for each amount of decrease in the temperature (-ΔT). The spacing coefficient between the patterns before the transition is indicated by the orange squares and the spacing coefficient beyond the transition is indicated by blue triangles. Visually each of the Delta T samples is different from each other. The change in the spacing coefficient increases as the difference in delta T while cooling down increases.

On the other hand, figure 26C shows the samples undergoing a counter experiment. Initially, all the samples are placed at 20^{o}C. The time of transition is chosen to be 12 hours for this experiment. (Since very few bands are observed in 6 hours at 20^{o}C, we had to choose a longer time for this initial temperature). The experimental (figure 26C), results indicate that 12 hours is sufficient time for several bands to be observed also at higher temperatures. After 12 hours at 20 C, the samples are heated up to final temperatures of 30, 40, 50, and 60^{o}C creating temperature differences of 10, 20, 30, and 40^{o}C, respectively. Similarly, the spacing coefficient of patterns before and after the transition are plotted in figure 26B for each increase in the temperature (ΔT). The spacing coefficient between the patterns before the transition is indicated by the blue squares and

the spacing coefficient beyond the transition is indicated by orange triangles. In heating experiments, a significant increase in the spacing coefficient is observed (figure 25B). Visually, each of the samples is quite distinguishable from each other as well.

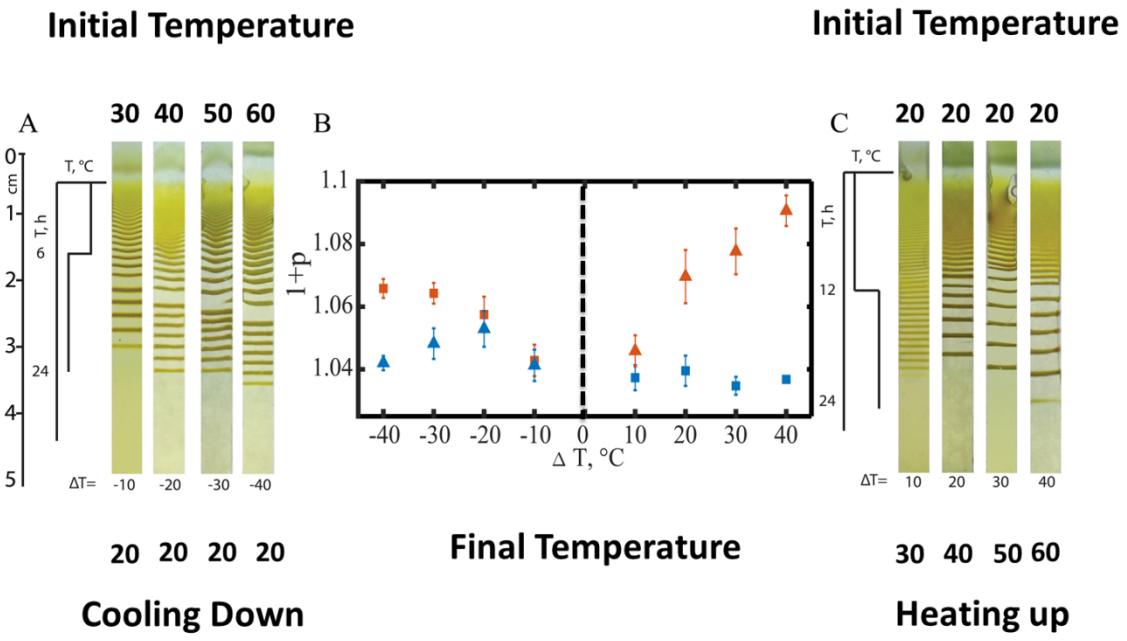

Figure 26: The effect of transition to different temperatures (transitions with different (-ΔT values) at a particular time of transition is shown. ΔT indicates the difference in temperature between pre- and post-transition times. (A) The samples are placed at higher temperatures (30, 40, 50, or 60^{o}C) for 6 hours (pre-transition time) and then cooled down to 20^{o}C. (B) Trend in spacing coefficient with respect to change in temperature: orange indicating higher temperatures, blue indicates 20oC for both A and C. Triangle represents 1+p after transition and square represents 1+p before transition. (C) The samples are placed at 20oC for 12 hours (pre-transition time) and then the sample is heated to higher temperatures (30, 40, 50, or 60^{o}C).

To summarize the results, we have quantified the effect of a magnitude of the change in temperature on LPs. The results show that LPs evolve visually and mathematically in a distinctive manner from each other in terms of transition time and the extent of temperature change. Previously, we have shown that the time of the transition is a degree

of freedom towards controlling periodic precipitation through temperature. Here, we showed that another degree of freedom is provided by the magnitude of temperature change. These results suggest the magnitude of delta T, which can be attributed as 'the amount of force' that we have in our hands for engineering the spacing and widths of periodic precipitation patterns.

3.4.3. Ramping the Temperature

So far, we have focused on finding factors influencing LPs under different temperature profiles. These included the extent of temperature change and the time of transition. Now we move towards considering the effect of rate at which the temperature of the gels is changed. Three ramps are chosen for the study to illustrate the effect of altering the temperature of the system. Temperature is varied between 20^{o}C and 50^{o}C or vice versa at 0.1, 1 and 10^{o}C/min. Subsequently, the transition time between changing temperature is 5 hours (300 min), 0.5 hour (30 min) and 3 min for 0.1, 1 and 10^{o}C/min ramping rates, respectively. The overall experiment takes 24 hours in all cases. For heating up, the system is kept at 20^{o}C for 17 hours and temperature is then varied at a set rate to 50^{o}C and kept at 50^{o}C till the 24^{th} hour. For cooling down, the system temperature is dropped to 20^{o}C at set rate after the 7^{th} hour of being kept at 50^{o}C.

Figure 27 quantifies the effect of ramping down temperature on spacing and widths of LPs. These results indicate that ramp rate is setting a guideline for the spontaneously occurring patterns. The general trends in spacing coefficient follows our expectations based on data retrieved from constant temperature experiments. The 1+p value increases when temperature is increased and lower values are obtained at lower temperatures (figure 27B). The widths of the patterns are following a similar trend as spacing coefficient i.e. post-transition patterns are getting narrower than pre-transition patterns, before blue arrow, or mid-transition patterns indicated by green arrow (figure 27C).

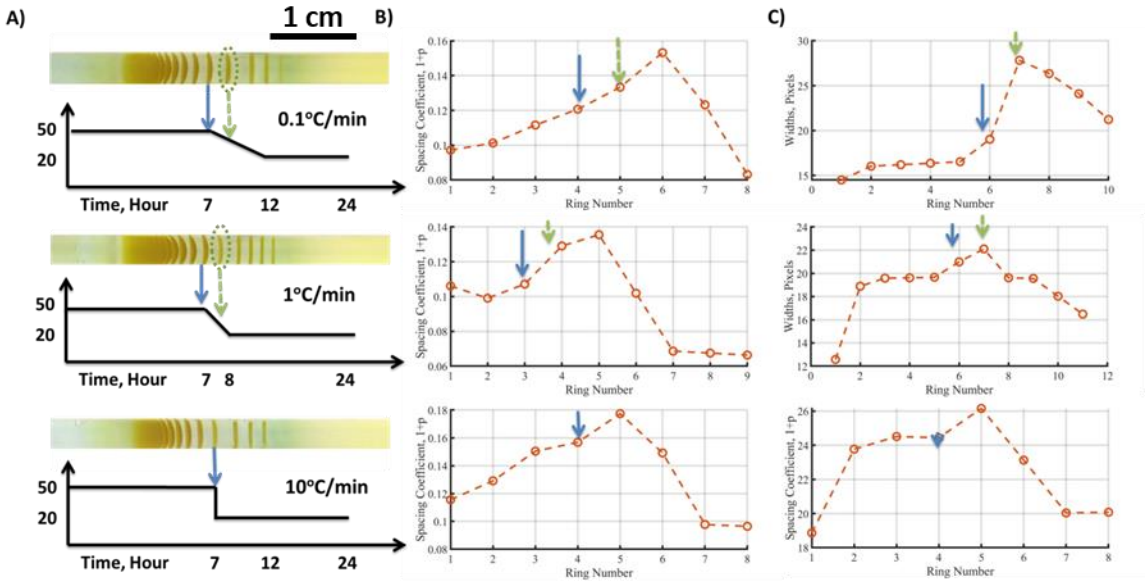

Figure 27: (A) Ramping down from 50 to 20 degree Celsius at 0.1, 10 and 10^{o}C/min from top to bottom. (B) The spacing coefficient variation with respect to the ring number for each of the ramp rate. (C) The widths of the patterns formed with respect to the ring number. Blue arrow indicating the point of transition and the green arrow represents the pattern formed during the transition period.

Figure 28 quantifies the effect of ramping up temperature on spacing and widths of LPs. The spacing coefficient and widths of the patterns demonstrate the difference between pre and post- transition patterns (figure 28B and 28C). It is expected to observe a sudden increase in the depletion zones as the temperature is getting higher. For 10^{o}C/min, there is a sudden rise in the width of the first post-transition patterns and following this the widths fall and tend to increase afterwards. It is observed that pattern formation is being affected by the rate at which temperature is changed. The main visual difference occurs in terms of the last band formed. Last band forms further in spatial coordinate for 0.1^{o}C/min while ramping down, and 10^{o}C/min while ramping up.

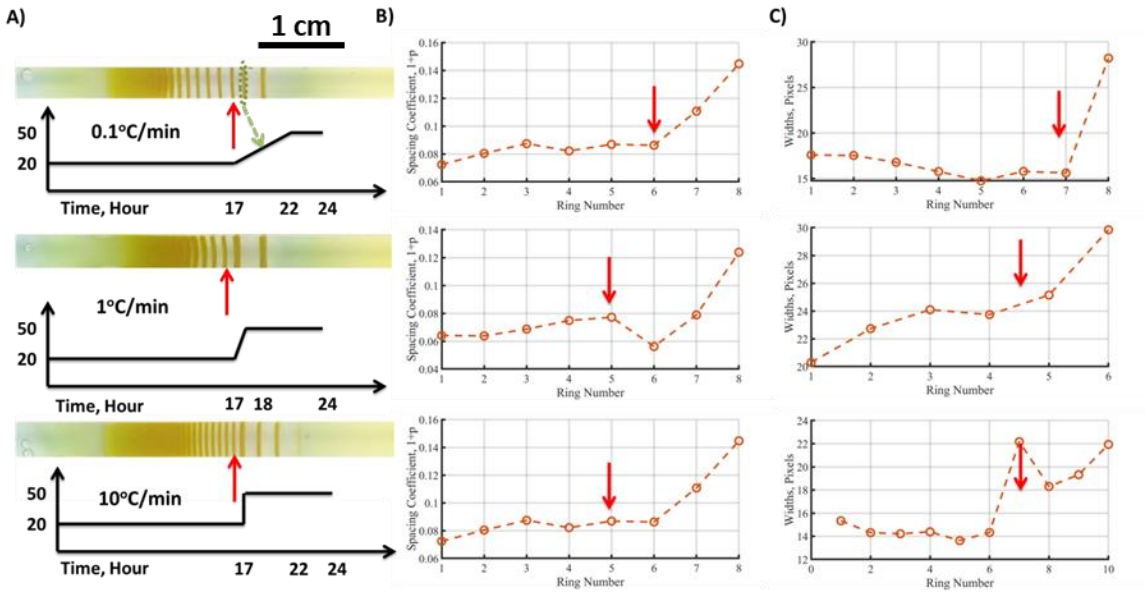

Figure 28: (A) Ramping up from 20 to 50 degree Celsius at 0.1, 10 and 10^{o}C/min from top to bottom. Scale bar is 1 cm. (B) The spacing coefficient variation with respect to the ring number for each of the ramp rate. (C) The widths of the patterns formed with respect to the ring number. Red arrow indicating the point of transition and the green arrow represents the pattern formed during the transition period.

Ramping temperature with different slopes does also effect pattern formation in a different way. Figure 29 indicates the space-time relationship of LPs undergoing different ramps. It is expected that at higher temperatures the slope of space-time plot of LPs increases (see figure 17). The relationship between the position of LPs and time at which they evolve is linear. However, when temperature is altered pattern formation undergo a deviation from the general set of rules. In terms of time law, this refers to the deviation from the linear relationship. It is observed that the slopes of pre- and post-transition patterns are different from each other in the same sample. In the case of ramping up (heating), the slope of the graph increases. In case of ramping down, the slope of the graph decreases in post-transition patterns. Furhtermore, the extent of change in the slope from pre- to post-transtion patterns is governed by the ramp rate. Ramping down at 0.1^{o}C/min gives the gradual post-transition slope, while 10^{o}C/min provides with the least steep post-transition slope. Ramping up experiments follow the exact opposite trend i.e.

10^{o}C/min provides the steepest post-transition slope, while 0.1^{o}C/min provides gradual post-transition slope.

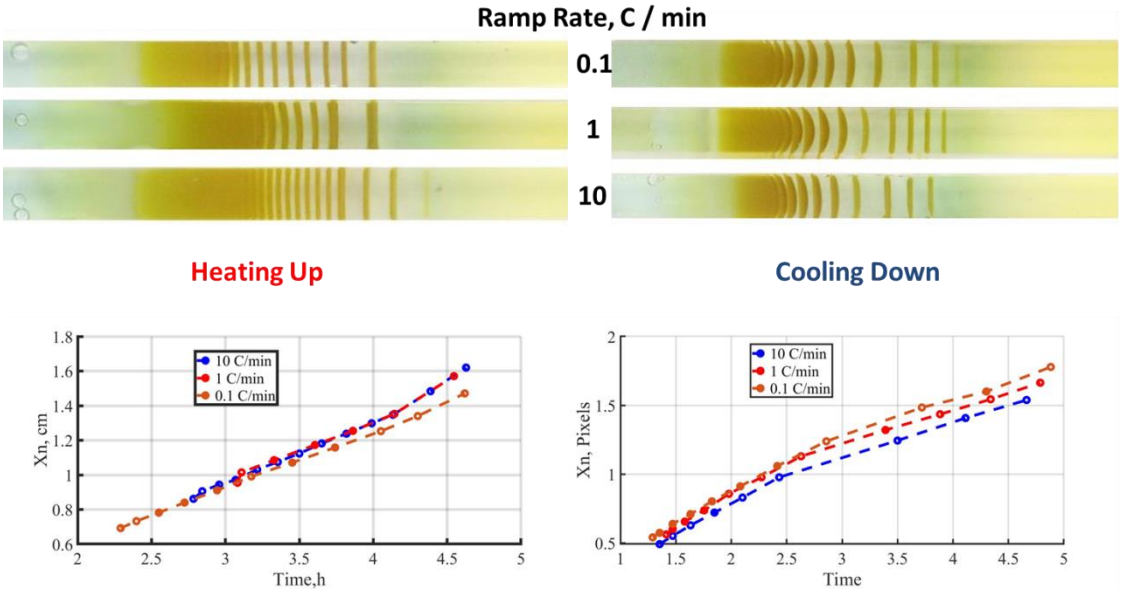

Figure 29: The variation in the space-time evolution of patterns in samples with difference in ramping rate of temperature change. (Right) Samples are placed at 20^{o}C for 17 hours and then temperature is increased to 50^{o}C at ramp rates of 0.1, 1 and 10^{o}C/min and then temperature is fixated at 50^{o}C till 24^{th} hour of the experiment. (Left) Samples are placed at 50^{o}C for 7 hours and then temperature is decreased to 20^{o}C at ramp rates of 0.1, 1 and 10^{o}C/min and then temperature is fixated at 20^{o}C till 24^{th} hour of the experiment. Space-time plots show the change in pattern evolution over time for different initial conditions and ramps.

It is certain that ramping temperature at different rates does alter the course of period precipitation patterns. A ramp acts as a guiding field for the patterns occurring in the post-transition regime. It is concluded already that LPs provide visual feedback for the time at which temperature change occurred, the extent of temperature change and now, the rate at which the temperature changes are visually distinguishable. In all above experiments, the empirical laws governing LPs are shown to be a function of temperature. When pulsating a system at different times, with different force or a

different rate, LPs show two regimes and each of the regimes follows the empirical laws of that temperature.

The evolution of the patterns when subjected to a change in temperature can be understood using the triangular relationship between k_p, k_d and K_{sp} and pushed and pulled fronts. Firstly, let's dissect a theoretical approach proposed by Antal et al. for such a forced manipulation of an LP system. In their work, they suggested a diffusive guiding field, originating from one end could result in inverse and equidistant banding [43]. Guiding field could be a temperature gradient such that the reaction front gets cooled down as it propagates through the system. As a result, the front propagates slowly as it moves along the temperature field and after certain point patterns form with decreasing distances between them (inverse banding). This is an example of coherent patterns forming behind a pulled reaction front. In our experimental conditions, a pulled reaction front occurs when temperature is lowered at a specific time and additionally, we also pull the reaction front at a specific rate as well. Even though our system lacks a temperature gradient across the gel, our results indicate manipulation of patterns and occurrence of localized inverse banding. This is observed in terms of the decrease in the spacing coefficient (figure 27B). Pulling a front means lowering the diffusion coefficient of copper ions and thus, slowing down the flux of copper ions. At the same instant, the solubility product of copper(II) chromate decreases and the precipitation threshold is lowered, along with, the rate constant. With all three integral components of the equation lowered, LPs transition to a lower temperature regime. A halt in the supply of the copper ions from the source results in a wider depletion zone beyond the last pre-transition band formed. As the front moves slowly and lowered reaction rate, results in lower production of colloids, their dissolution, re-precipitation and aggregation. With the lowered precipitation threshold, it is expected to see a continuous precipitation beyond pre-transition patterns and before post-transition patterns; however such a visual change is not observed. In this scenario, k_p, and k_d dominate over K_{sp}. Instead, a wide band appears as the first post-transition band. The width of this band indicates aggregation of a higher number of colloids to form a band. Additionally, this wider band requires higher time interval to form, and thus, lowers the slope of space-time plot (figure 29). This increased

time interval refers to the relaxation time due to a pulled front. Now we can also discuss the effect of ramp rate on the relaxation time of the system. In case of ramping temperature down, the relaxation time is higher for a sudden temperature change (10^{o}C/min) compared to a gradual change in the system's temperature (0.1^{o}C/min). Thus, the slopes of cooling down LP system (figure 29) demonstrate such trend. Later on, the spacing between post-transition bands starts to increase, however, the increase in not comparable to pre-transition patterns formed at higher temperatures (figure 27). Thus, the system relaxes after the perturbation in the form of a pulled front and returns to its normal characteristics.

Perturbing the system by heating up results in an increase in k_p, k_d and K_{sp} and a pushed front. In case of the pushed front, the flux of the copper ions from the source increases. The reaction rate constant indicates that all parts of the complex chain of events leading to periodic precipitation patterns i.e. formations of colloids, their dissolution, re-precipitation as bigger colloids and aggregation into a periodic band structure occur at a higher rate. Thus, bands start to occur immediately upon the rise in temperature. At this point the k_p and k_d dominate over K_{sp}, because if K_{sp} had dominated an immediate ring would not be observed and wider depletion zone would have been observed. The raised solubility product adds to the fact that wider depletion zones are observed post-transition patterns. With a pushed front, the system does not undergo a relaxation period and that is why the slopes of the space-time plots for post-transition patterns increase. Similarly, the rate at which temperature changes effects the extent of a pushed front and thus faster moving fronts (10^{o}C/min) will provide with steeper slopes.

3.4.4. Band Bending

LPs demonstrate visual differences when cooled down or heated up. The experiments were continuously monitored for discovering the whether any changes arise in pattern shape. Surprisingly, a new trend is observed when the temperature varied which is previously not reported in literature. Figure 30 illustrate how conventionally known as stationary LPs demonstrate dynamic behavior upon changing temperature. The patterns

appear to undergo a slight motion when subjected to a certain change in temperature. Upon keeping the temperature constant, patterns appear to be stationary and no motion is expected out of them. However, ramping experiments uncover the possibility of making LPs dynamic. For the later discussion outward bending refers to the bending patterns in a forward direction with respect to the direction of the moving copper front and inward bending refers to the backward bending of patterns opposite to the propagation reaction front. Upon increasing the temperature of the system, the already formed periodic precipitation patterns (pre-transition patterns) undergo an inward bending. And while cooling the system down, pre-transition LPs undergo forward bending. Here we could argue, that a reaction diffusion system possesses a certain inertia. And as the subjected to the laws of inertia, upon acceleration there is back-pull to resist the change in inertia and while decelerating there is front push in resistance to change in the inertia. Heating up the system leads to a pushed front and patterns seemingly demonstrate an inward bending. While cooling down, leads to pulled front and patterns undergo an outward bending. Patterns forming behind the reaction front show an inertial connection with the front.

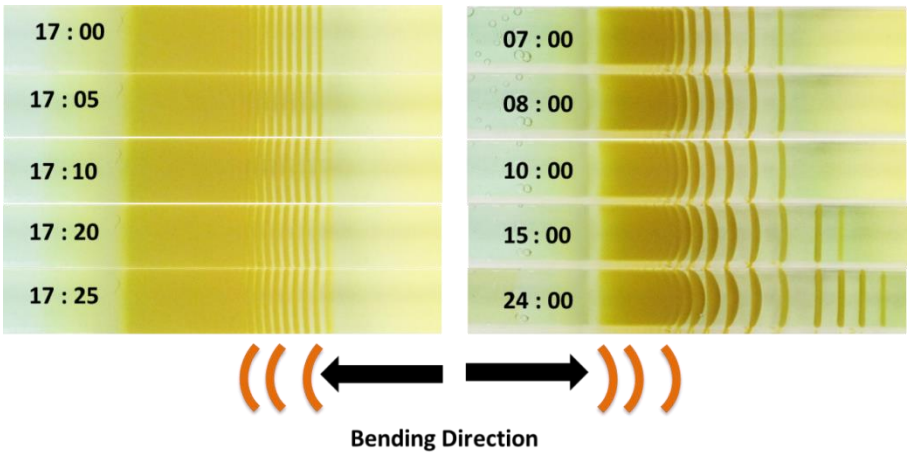

Figure 30: The time lapse beyond the transition point towards heating (left) and cooling (right). The direction of bending observed in patterns is demonstrated to be backwards when the system is heated up and forward when the system is cooled down. The time is displayed in hours: minutes. For heating up (left) transition takes place 17^{th} hour while for cooling down (right) the transition takes place at 7^{th} hour.

Another possibility for this phenomenon to occur is to account for the occurrence of deformation in the gel. As argued earlier copper ions do possess the ability to create a deformation in the gel by dint of complexation with the gel. Or the gel can undergo deformations upon a change in temperature. In both cases (deformation or inertia), pattern bending should be reversible. As in patterns forming in a certain deformed geometry should return to the original shape, when the load is applied again. And the state of the system will always resist a change.

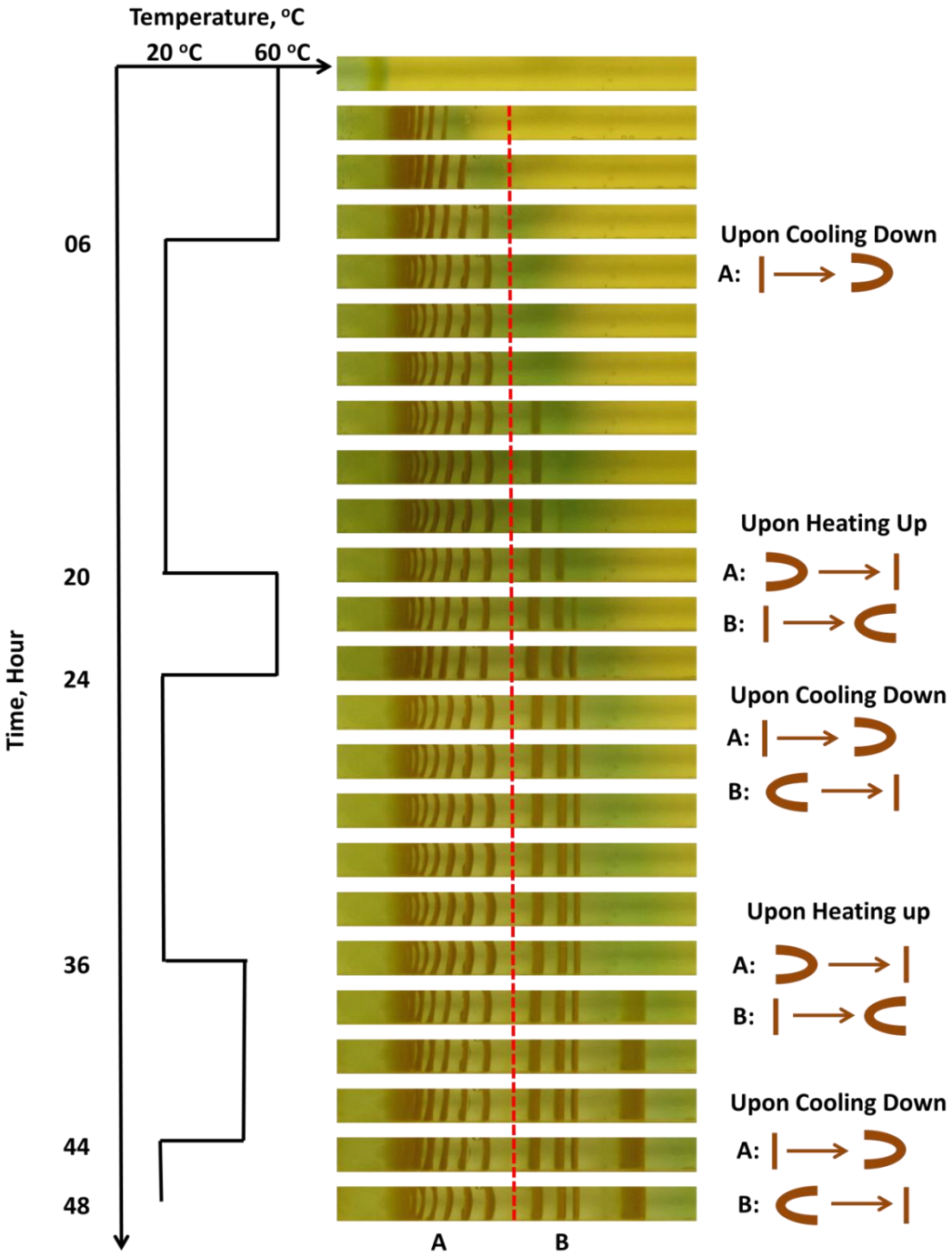

Figure 31: Periodic precipitation patterns are allowed to form in temperature conditions (shown left). Patterns are divided into two subclasses A (Patterns formed at 60oC) and B (Patterns formed at 20oC). The instances where a change in bending of patterns A and B starts is illustrated (right)

Figure 31 shows that pattern bending is reversible. Here, three steps of temperature change are introduced to the system in the form of lowering the temperature and each step varies in terms of its duration. First step occurs at 6^{th} hour and temperature is lowered to $20^{o}C$ from $60^{o}C$. Till 20^{th} hour, the pre-transition patterns (A) undergo an outward bending. After the end of first step (20^{th} hour), patterns return to the initial shape. And the post-transition patterns (B) show an inward bending. At beginning of step 2 (24^{th} hour), A patterns start to undergo outward bending while B patterns return to their initial position. And at the end of step 2 (36^{th} hour), A patterns begin to achieve their initial shape while B patterns undergo inward bending. Similar trend is shown at the beginning and end of step 3 (44^{th} hour). The extent of bend is similar at each beginning or ending of the step. This makes us sure that no dissolution bands or formation of more copper(II) chromate on to the periodic bands occurs. Thus, band bending is reversible and reproducible. This observation also makes LPs technologically more relevant for visual temperature measurements.

3.4.5. SEM analysis of samples undergoing temperature changes

We have shown that temperature governs the empirical laws defining LPs along with visually distinct patterned hydrogels are formed. With temperature as a degree of freedom, widths, spacing and time of patterns can be tuned. We have also shown that size of particles in a specific band is higher at hotter conditions. Now we progress to discuss the effect of a thermal pulse to the particle size in a band. Figure 32 shows a pattern forming system kept at $20^{o}C$ for 17 hours, ramped at $1^{o}C$/min to $60^{o}C$ and then temperature is maintained at $60^{o}C$ till 24^{th} hour. There is a total of 9 rings formed. Ring 1 to 7 form at $20^{o}C$, ring 8 forms during the ramp up and ring 9 forms at $60^{o}C$. From the SEM images and the histograms, it is observed that from ring 1 to 7 particle size increases and it is similar to the pattern at $20^{o}C$ (figure19 and 20). Ring 8 however demonstrates particles with huge distribution in terms of their particle size. As ring 8 forms while temperature is being ramped to $60^{o}C$, particles with both smaller and larger

particle sizes are observed. Ring 9 shows a very big jump in particle size, corresponding to the particle sizes obtained late in constant 60°C sample.

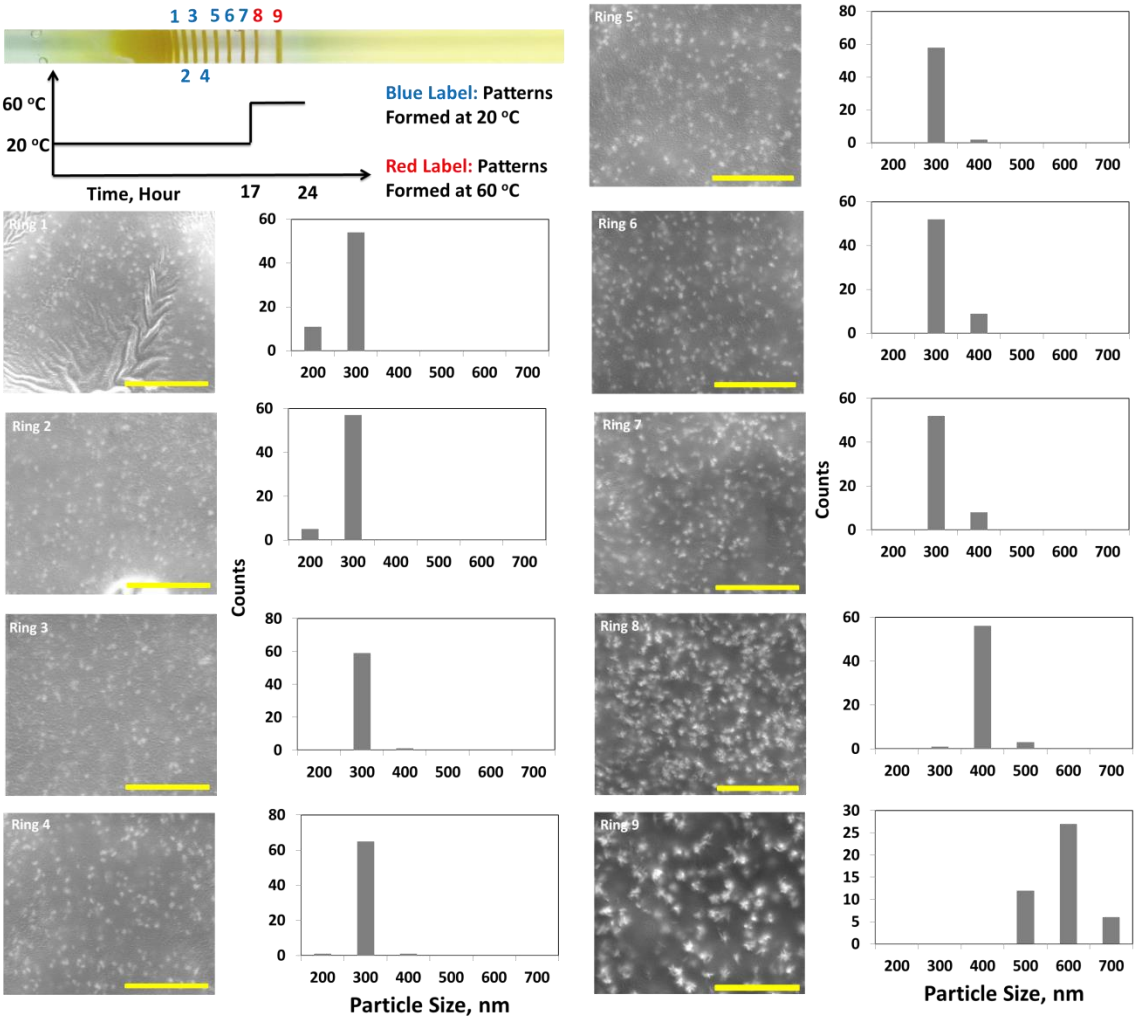

Figure 32: Patterns are formed in a sample with temperature variations from 20 to 60°C. Patterns formed at 20°C are highlighted with blue and patterns formed at 60°C are highlighted with red. The SEM images are for rings 1 to 9 with histograms on their right showing the distribution of particle size. The scale bar (yellow line) represents 5 µm.

In an alternate experiment (figure 33), the system is allowed to form LPs at 60°C for 6 hours, ramped at 1°C/min to 20°C and then temperature is kept constant at 20°C till 24th hour. A total of 10 rings are formed in this experiment. Rings 1 to 6 form at 60°C, ring 7 to 10 form at 20°C and no ring forms in the duration of ramping down temperature. From ring 1 to 6 the particle size increases and in ring 6 we observe large particles. Ring 7 is

the first pattern forming at 20°C. We observe the sizes of the particles show a sharp fall as compared to ring 6. The effect is also visible from big, bright spots in ring 6 to small, tiny spots in ring 7. Following ring 7, the particle size starts to increase again in ring 8 and 9. The distribution of particle size is not high in ring 10 but it is due to the fact that the ring formation is not complete.

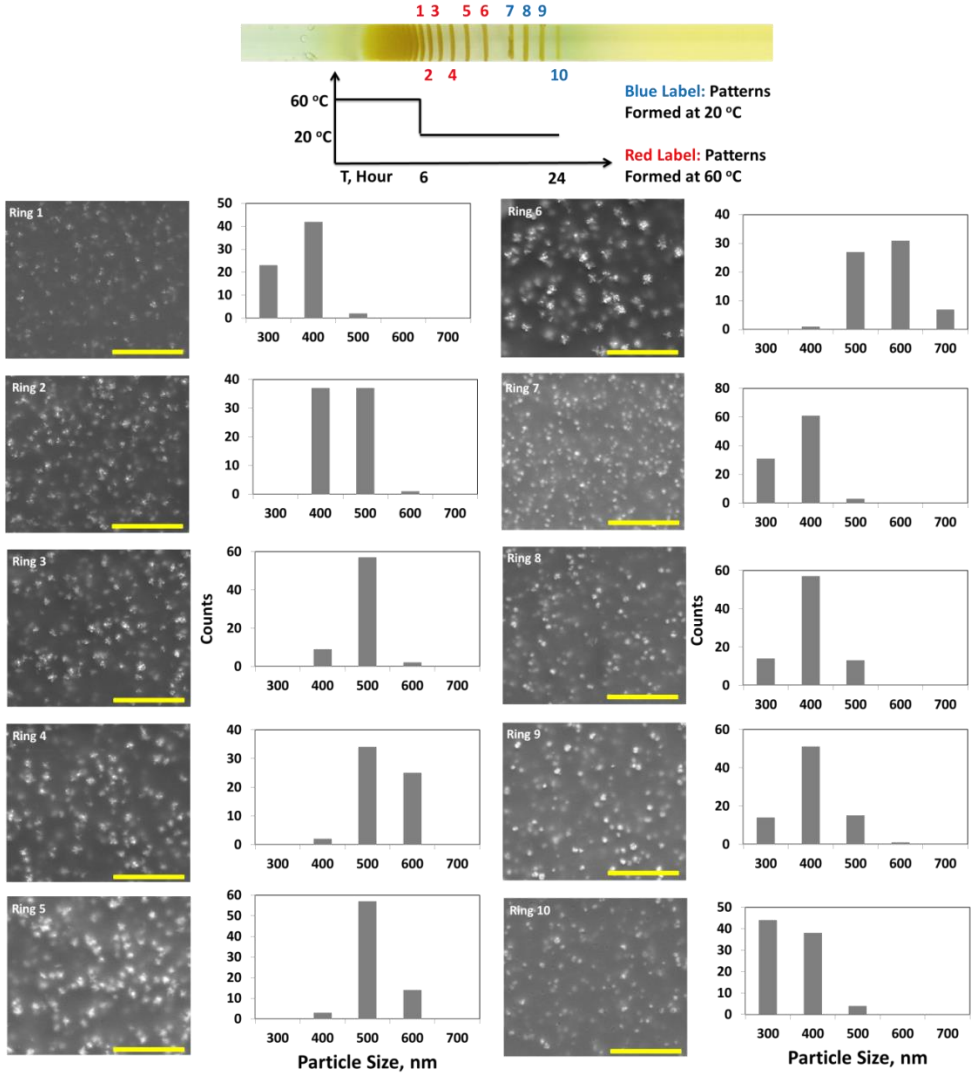

Figure 33: Patterns are formed in a sample with temperature variations from 60 to 20°C. Patterns formed at 20°C are highlighted with blue and patterns formed at 60°C are highlighted with red. The SEM images are for rings 1 to 10 with histograms on their right showing the distribution of particle size. The scale bar (yellow line) represents 5 µm.

From these results it is concluded that particle size is highly dependent upon the temperature of the system and the change in temperature effects the size of the particles in the post-transition rings. As a known fact, particle size increases along the spatial coordinate in LPs[38]. With these observations, for the first time, we show that the trend of particle size can be altered by varying the temperature of the system. The particle size can be increased or decreased at the desired ring, time and space using temperature.

3.5. Thermally Probing LPs in different dimensions

Up to now, we have shown that the pattern evolution is affected by the direction, magnitude, time, and steepness of the temperature step. We have also shown the characteristics of patterns forming in pre and post-transition times. It has been made clear that the shape, widths, spacing, and the time of pattern formation can be controlled by temperature, along with, the particle size. Now we begin to pattern a hydrogel with cyclic temperature changes. An example of this cyclic change is given in the figure 30. The steps are of equal magnitude but of different duration. Here in figure 34A, we show another sample undergoing cyclic temperature changes however with different thermal profile. The instances of change in temperature are visually observable from the spacing between the patterns. The changes undergone by the spacing coefficient and widths of the patterns along the thermal profile are shown in figure 34D and 34E.

So far, our experiments were limited to 1D diffusion of the copper front. Now we see that pattern LPs are being affected in a similar fashion in 2D system by temperature (figure 34B). This clarifies the fact that surface area of 1D gel is not playing a crucial role in the above observations. The spacing between the patterns decreases upon an increase in temperature. And similarly, wider depletion zones are observed upon lowering of temperature. The trend in spacing and widths of the patterns along the thermal profile is also indicated in figure 34D and 34E. We have shown that LPs can be controlled and altered by temperature in a 2D setup as well. At this point, the similarity between synthetic LPs and tree rings (figure 3) becomes clearer. As the study of the tree rings indicates the seasonal temperature changes by dint of the spacing between the patterns,

here we have shown an artificial system that senses environmental temperature changes using concurrent pattern formation.

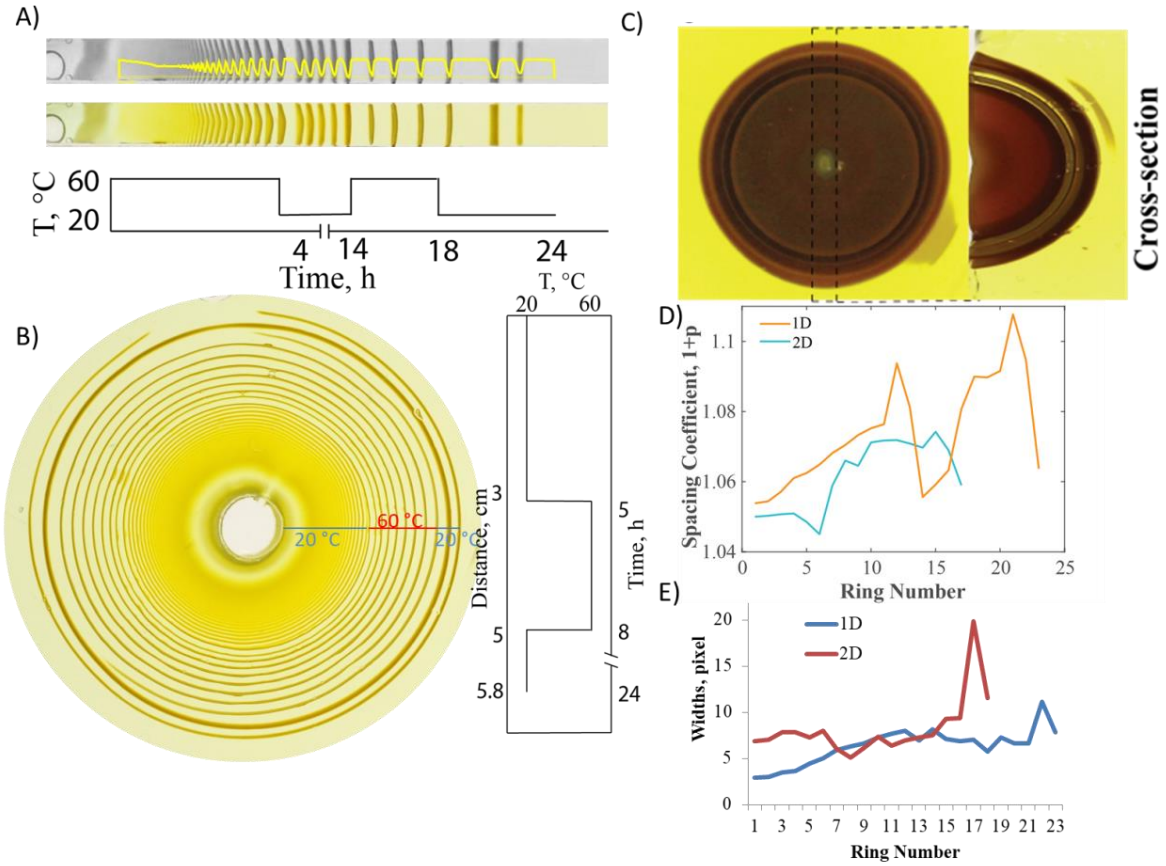

Figure 34: A) Cyclic temperature oscillations between 60 and 20°C encoded within the visual appearance of the patterns in 1 D sample. Initially kept at 60oC for 4 hours and then transferred to 20°C for the next 10 hours. At 14th hour the sample is replaced into the 60°C for 4 hours and then temperature is lowered to 20°C till the 24th hour. B) Cyclic temperature changes in a 2D sample. With the plot illustrating the difference in the time evolution of the patterns in comparison to the spatial distance covered by LPs at two different temperatures. C) Cyclic temperature changes in a 3D sample. A cross-section of 3D patterns (Z-axes). D) The effect of changing the temperature on the spacing coefficient and widths (E) of patterns formed in A) and B).

Finally, the LPs-temperature dependence is also demonstrated in 3D (figure 34C). The cross-sectional view represents a cut in the middle of the 3D gel block along the added z-axis. It is clearly visible that the spacing between patterns rises, falls and a wider band

forms. Thus, altering the three factors (diffusion coefficient, precipitation threshold, and reaction rate) alters the course of LPs in all possible dimensions for diffusion. LPs can be engineered in the most similar fashion to nature by dint of a varying thermal profile. Also, the thermal profile can be tracked in the visual appearance of the patterns, making LPs suitable for long-term environmental temperature trackers.

4. Conclusion

The relationship between Liesegang patterns (LPs) and temperature is studied in a quantitative fashion. LPs are visual sums of complex events governed by reaction rate, diffusion coefficient, and solubility product. These factors are individually affected by temperature. Thus, LPs demonstrated differences in their appearance and mathematical functions with respect to temperature of the system. It is shown that diffusion coefficient of copper ion in polyacrylamide matrix increases with temperature. The reaction rate between copper ions and chromate ions also increases with temperature. Finally, solubility product of copper(II) chromate increases as well with temperature. As a result, LPs occur faster with wider depletion zones at higher temperatures.

It is concluded that thermal wave can be tracked in the visual appearance of the patterns. LPs show distinct behaviors upon undergoing a transition in temperature. This distinction occurs due to a wide range of factors including, the time of transition, extent of temperature change and the rate at which the temperature is changed. Two distinct observations are made when LPs are transition to a different temperature. Upon cooling down, a wide depletion zone occurs followed by a dip in the spacing and widths of the patterns. Upon heating up, a narrow depletion zone occurs followed by an increase in the spacing and widths of the patterns. The relationship between diffusion coefficient, reaction rate and solubility product and their effect is explained upon temperature changes.

A new observation is brought to light when temperature of the system is altered. Band bending occurs after the systems temperature is changed. An outward bend is observed for lowering temperature and inward bending occurs upon increasing temperature. Band bending is shown to be reversible. This also makes LPs a good candidate for long-term non-contact temperature tracking.

Additionally, the particle size is observed to increase in a simultaneous ring at a higher temperature. Upon transitioning temperature, the particle sizes also alter i.e. decrease in case of lowering temperature and increase when temperature is increased. Thus, the general trend in particle sizes can be altered using temperature.

5. References

[1] J. A. S. Kelso, "Dynamic patterns: The self-organization of brain and behavior," *Complexity*, vol. 2, no. 3, pp. 45–46, 1997.

[2] B. A. Grzybowski, *Chemistry in Motion. Reaction–Diffusion Systems for Micro- and Nanotechnology*. 2009.

[3] P. Jung, A. Cornell-Bell, F. Moss, S. Kadar, J. Wang, and K. Showalter, "Noise sustained waves in subexcitable media: From chemical waves to brain waves," *Chaos*, vol. 8, no. 3, pp. 567–575, 1998.

[4] H. K. Henisch, *Crystals in Gels and Liesegang Rings*. .

[5] R. M. Walliser *et al.*, "Growth of nanoparticles and microparticles by controlled reaction-diffusion processes," *Langmuir*, vol. 31, no. 5, pp. 1828–1834, 2015.

[6] M. Saad, A. Safieddine, and R. Sultan, "Revisited Chaos in a Diffusion-Precipitation-Redissolution Liesegang System," *J. Phys. Chem. A*, vol. 122, no. 29, pp. 6043–6047, 2018.

[7] I. Lagzi, B. Kowalczyk, and B. A. Grzybowski, "Liesegang rings engineered from charged nanoparticles," *J. Am. Chem. Soc.*, vol. 132, no. 1, pp. 58–60, 2010.

[8] R. F. Sultan and A. F. M. Abdel-Rahman, "On dynamic self-organization: Examples from magmatic and other geochemical systems," *Lat. Am. J. Solids Struct.*, vol. 10, no. 1, pp. 59–73, 2013.

[9] E. C. H. Davies, "Liesegang rings. II. Rhythmic bands of dyes on filter paper and cloth by evaporation. The refractivity, surface tension, conductivity, viscosity, and brownian movement of dye solutions," *J. Am. Chem. Soc.*, vol. 44, no. 12, pp. 2705–2709, 1922.

[10] I. Ferenc and I. Lagzi, "Models of Liesegang pattern formation," vol. 661, no. 2, p. 10, 2010.

[11] Z. Rácz, "Formation of Liesegang patterns," vol. 274, pp. 50–59, 1999.

[12] H. W. Morse and G. W. Pierce, "Diffusion and Supersaturation in Gelatin," *Phys. Rev.*, vol. XVII, no. 3, 1903.

[13] Z. Rácz, "Formation of Liesegang patterns," *Phys. A Stat. Mech. its Appl.*, vol. 274, no. 1, pp. 50–59, 1999.

[14] P. S. Kulkarni, "Revert Banding in One-Dimensional Periodic Precipitation of the

(AgNO 3 + KBr) System in Agar Gel," no. 1, 2019.

[15] H. W. Morse and G. W. PIERCE., "DIFFUSION AND SUPERSATURATION IN GFLATINE. BY," *Phys. Rev.*, vol. XVII, no. 3, pp. 129–150, 1903.

[16] M. Morsali, M. Turab, A. Khan, R. Ashirov, and G. Holló, "Mechanical Control of Periodic Precipitation in Stretchable Gels to Retrieve Information on Elastic Deformation and for Complex Patterning of Matter," vol. 1905779, pp. 1–36, 2020.

[17] A. Lara and R. Villalba, "A 3620-year temperature record from Fitzroya cupressoides tree rings in southern South America," *Science (80-.).*, vol. 260, no. 5111, pp. 1104–1106, 1993.

[18] I. Lagzi, "Formation of Liesegang patterns in an electric field," no. April 2002, pp. 1–4, 2015.

[19] H. Hayashi, S. Aoki, and H. Abe, "Magnetic-Field-Induced Painting-Out of Precipitation Bands of Mn-Fe-Based Prussian Blue Analogues in Water-Glass Gels," *ACS Omega*, vol. 3, no. 4, pp. 4494–4501, 2018.

[20] K. Mohanan Pillai, V. K. Vaidyan, and M. A. Ittyachan, "Effect of Different Parameters on the Liesegang Ring Formation of Lead Carbonate Crystals," *Cryst. Res. Technol.*, vol. 17, no. 12, pp. 1529–1534, 1982.

[21] I. Lagzi and D. Ueyama, "Pattern transition between periodic Liesegang pattern and crystal growth regime in reaction-diffusion systems," *Chem. Phys. Lett.*, vol. 468, no. 4–6, pp. 188–192, 2009.

[22] M. Fiałkowski, A. Bitner, and B. A. Grzybowski, "Wave optics of liesegang rings," *Phys. Rev. Lett.*, vol. 94, no. 1, pp. 14–16, 2005.

[23] M. Orlik, "Introduction to the dynamic self-organization of chemical systems," *ChemTexts*, vol. 3, no. 3, pp. 1–41, 2017.

[24] M. Parsa, S. Harmand, K. Sefiane, M. Bigerelle, and R. Deltombe, "Effect of substrate temperature on pattern formation of nanoparticles from volatile drops," *Langmuir*, vol. 31, no. 11, pp. 3354–3367, 2015.

[25] T. Ban, M. Kaji, Y. Nagatsu, and H. Tokuyama, "Propagating Precipitation Waves in Disordered Media," *ACS Omega*, vol. 2, no. 11, pp. 8027–8032, 2017.

[26] N. Chevalier, "The influence of thermal noise on Liesegang pattern formation And

other related aspects of this remarkable," no. February, 2006.

[27] S. Thomas, I. Lagzi, F. Molnár, and Z. Rácz, "Probability of the emergence of helical precipitation patterns in the wake of reaction-diffusion fronts," *Phys. Rev. Lett.*, vol. 110, no. 7, 2013.

[28] T. Isemura, "Studies on Rhythmic Precipitates," *Bull. Chem. Soc. Jpn.*, vol. 57, no. 1, pp. 1–59, 1938.

[29] S. S. Das, "Chemical Instability and Periodic Precipitation of Copper Chromate in Gel Media Influence of Light on Precipitation Pattern Influence of Gravitational Field," vol. 130, no. 1, pp. 176–183, 1989.

[30] M. A. Han, S. H. Jun, and Y. Kang, "Effect of electrolyte on the shapes of Liesegang rings," *J. Korean Chem. Soc.*, vol. 52, no. 4, pp. 356–361, 2008.

[31] T. Morita, T. Narita, S. A. Mukai, M. Yanagisawa, and M. Tokita, "Phase behaviors of agarose gel," *AIP Adv.*, vol. 3, no. 4, 2013.

[32] T. Antal, M. Droz, J. Magnin, A. Pekalski, and Z. Rácz, "Formation of Liesegang patterns: simulations using a kinetic Ising model," *J. Chem. Phys.*, vol. 114, no. 8, pp. 3770–3775, 2001.

[33] T. Antal, I. Bena, M. Droz, K. Martens, and Z. Rácz, "Guiding fields for phase separation: Controlling Liesegang patterns," *Phys. Rev. E - Stat. Nonlinear, Soft Matter Phys.*, vol. 76, no. 4, pp. 1–9, 2007.

[34] I. Neamtu, A. P. Chiriac, and L. Nita, "Characterization of poly (acrylamide) as temperature- sensitive hydrogel," *J. Optoelectron. Adv. Mater.* ·, 2006.

[35] S. Thomas, I. Lagzi, F. Molnár, and Z. Rácz, "Helices in the wake of precipitation fronts," *Phys. Rev. E - Stat. Nonlinear, Soft Matter Phys.*, vol. 88, no. 2, 2013.

[36] C. Storm, W. Spruijt, U. Ebert, and W. Van Saarloos, "Universal algebraic relaxation of velocity and phase in pulled fronts generating periodic or chaotic states," *Phys. Rev. E - Stat. Nonlinear, Soft Matter Phys.*, vol. 61, no. 6, pp. 6063–6066, 2000.

[37] H. Nabika, M. Itatani, and I. Lagzi, "Pattern Formation in Precipitation Reactions: The Liesegang Phenomenon," *Langmuir*, vol. 36, no. 2, pp. 481–497, 2020.

[38] R. Zakhia Douaihy, M. Al-Ghoul, and M. Hmadeh, "Liesegang Banding for Controlled Size and Growth of Zeolitic-Imidazolate Frameworks," *Small*, vol. 15,

no. 28, pp. 1–6, 2019.

[39] R. M. Walliser *et al.*, “Growth of nanoparticles and microparticles by controlled reaction-diffusion processes,” *Langmuir*, vol. 31, no. 5, pp. 1828–1834, 2015.

[40] P. A. Korevaar, C. N. Kaplan, A. Grinthal, R. M. Rust, and J. Aizenberg, “Non-equilibrium signal integration in hydrogels,” *Nat. Commun.*, vol. 11, no. 1, 2020.

[41] C. COETZEE, “THE PREPARATION, SOLUBILITY AND MEAN ACTIVITY-COEFFICIENT OF COPPER CHROMATE,” *J. Inorg. Nucl. Chem.*, vol. 43, no. 2, pp. 417–418, 1981.

[42] G. H. Jeffery, J. Bassett, J. Mendham, and R. C. Denney, *Quantitative Chemical Analysis*, 5th ed. 1989.

[43] T. Antal, I. Bena, M. Droz, K. Martens, and Z. Rácz, “Guiding fields for phase separation: Controlling Liesegang patterns,” *Phys. Rev. E - Stat. Nonlinear, Soft Matter Phys.*, vol. 76, no. 4, pp. 1–9, 2007.

[44] M. Aksoy, S. V. K. Nune, and F. Karadas, “A Novel Synthetic Route for the Preparation of an Amorphous Co/Fe Prussian Blue Coordination Compound with High Electrocatalytic Water Oxidation Activity,” *Inorg. Chem.*, vol. 55, no. 9, pp. 4301–4307, 2016.

[45] D. Saliba, M. Ammar, M. Rammal, M. Al-Ghoul, and M. Hmadeh, “Crystal Growth of ZIF-8, ZIF-67, and Their Mixed-Metal Derivatives,” *J. Am. Chem. Soc.*, vol. 140, no. 5, pp. 1812–1823, 2018.

[46] J. H. Park, J. Paczesny, N. Kim, and B. A. Grzybowski, “Shaping Microcrystals of Metal–Organic Frameworks by Reaction–Diffusion,” *Angew. Chemie - Int. Ed.*, pp. 1–6, 2020.